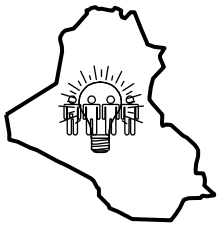

SPONSORED AND PUBLISHED BY
THE IRAQI SOCIETY FOR ALTERNATIVE AND RENEWABLE ENERGY SOURCES AND TECHNIQUES (I.S.A.R.E.S.T.)

EDITORIAL BOARD

ADVISORY BOARD

ISSN 1813-2065

All NOBEL Laureates in Physics

Edited by
Oday A. Hamadi
P. O. Box 55159,
Baghdad 12001, Iraq

The Nobel Prize Awarders

Who selects the Nobel Laureates? In his last will and testament, Alfred Nobel specifically designated the institutions responsible for the prizes he wished to be established: The Royal Swedish Academy of Sciences for the Nobel Prize in Physics and Chemistry, Karolinska Institute for the Nobel Prize in Physiology or Medicine, the Swedish Academy for the Nobel Prize in Literature, and a Committee of five persons to be elected by the Norwegian Parliament (Storting) for the Nobel Peace Prize. In 1968, the Sveriges Riksbank established the Sveriges Riksbank Prize in Economics in Memory of Alfred Nobel. The Royal Swedish Academy of Sciences was given the task to select the Economics Prize Laureates starting in 1969.
The Nobel Prize in Physics has been awarded to 180 individuals since 1901. (John Bardeen was awarded the prize in both 1956 and 1972). Would like to introduce them? Let's go…

- 1901 - Wilhelm Conrad Röntgen
- 1902 - Hendrik A. Lorentz, Pieter Zeeman
- 1903 - Henri Becquerel, Pierre Curie, Marie Curie
- 1904 - Lord Rayleigh
- 1905 - Philipp Lenard
- 1906 - J.J. Thomson
- 1907 - Albert A. Michelson
- 1908 - Gabriel Lippmann
- 1909 - Guglielmo Marconi, Ferdinand Braun
- 1910 - Johannes Diderik van der Waals
- 1911 - Wilhelm Wien
- 1912 - Gustaf Dalén
- 1913 - Heike Kamerlingh Onnes
- 1914 - Max von Laue
- 1915 - William Bragg, Lawrence Bragg
- 1916 - The prize money was allocated to the Special Fund of this prize section
- 1917 - Charles Glover Barkla
- 1918 - Max Planck
- 1919 - Johannes Stark
- 1920 - Charles Edouard Guillaume
- 1921 - Albert Einstein
- 1922 - Niels Bohr
- 1923 - Robert A. Millikan
- 1924 - Manne Siegbahn
- 1925 - James Franck, Gustav Hertz
- 1926 - Jean Baptiste Perrin
- 1927 - Arthur H. Compton, C.T.R. Wilson
- 1928 - Owen Willans Richardson
- 1929 - Louis de Broglie
- 1930 - Sir Venkata Raman
- 1931 - The prize money was allocated to the Special Fund of this prize section
- 1932 - Werner Heisenberg
- 1933 - Erwin Schrödinger, Paul A.M. Dirac
- 1934 - The prize money was with 1/3 allocated to the Main Fund and with 2/3 to the Special Fund of this prize section
- 1935 - James Chadwick
- 1936 - Victor F. Hess, Carl D. Anderson
- 1937 - Clinton Davisson, George Paget Thomson
- 1938 - Enrico Fermi
- 1939 - Ernest Lawrence
- 1940 - The prize money was with 1/3 allocated to the Main Fund and with 2/3 to the Special Fund of this prize section
- 1941 - The prize money was with 1/3 allocated to the Main Fund and with 2/3 to the Special Fund of this prize section
- 1942 - The prize money was with 1/3 allocated to the Main Fund and with 2/3 to the Special Fund of this prize section
- 1943 - Otto Stern
- 1944 - Isidor Isaac Rabi
- 1945 - Wolfgang Pauli
- 1946 - Percy W. Bridgman
- 1947 - Edward V. Appleton

- 1948 - Patrick M.S. Blackett
- 1949 - Hideki Yukawa
- 1950 - Cecil Powell
- 1951 - John Cockcroft, Ernest T.S. Walton
- 1952 - Felix Bloch, E. M. Purcell
- 1953 - Frits Zernike
- 1954 - Max Born, Walther Bothe
- 1955 - Willis E. Lamb, Polykarp Kusch
- 1956 - William B. Shockley, John Bardeen, Walter H. Brattain
- 1957 - Chen Ning Yang, Tsung-Dao Lee
- 1958 - Pavel A. Cherenkov, Il´ja M. Frank, Igor Y. Tamm
- 1959 - Emilio Segrè, Owen Chamberlain
- 1960 - Donald A. Glaser
- 1961 - Robert Hofstadter, Rudolf Mössbauer
- 1962 - Lev Landau
- 1963 - Eugene Wigner, Maria Goeppert-Mayer, J. Hans D. Jensen
- 1964 - Charles H. Townes, Nicolay G. Basov, Aleksandr M. Prokhorov
- 1965 - Sin-Itiro Tomonaga, Julian Schwinger, Richard P. Feynman
- 1966 - Alfred Kastler
- 1967 - Hans Bethe
- 1968 - Luis Alvarez
- 1969 - Murray Gell-Mann
- 1970 - Hannes Alfvén, Louis Néel
- 1971 - Dennis Gabor
- 1972 - John Bardeen, Leon N. Cooper, Robert Schrieffer
- 1973 - Leo Esaki, Ivar Giaever, Brian D. Josephson
- 1974 - Martin Ryle, Antony Hewish
- 1975 - Aage N. Bohr, Ben R. Mottelson, James Rainwater
- 1976 - Burton Richter, Samuel C.C. Ting
- 1977 - Philip W. Anderson, Sir Nevill F. Mott, John H. van Vleck
- 1978 - Pyotr Kapitsa, Arno Penzias, Robert Woodrow Wilson
- 1979 - Sheldon Glashow, Abdus Salam, Steven Weinberg
- 1980 - James Cronin, Val Fitch
- 1981 - Nicolaas Bloembergen, Arthur L. Schawlow, Kai M. Siegbahn
- 1982 - Kenneth G. Wilson
- 1983 - Subramanyan Chandrasekhar, William A. Fowler
- 1984 - Carlo Rubbia, Simon van der Meer
- 1985 - Klaus von Klitzing
- 1986 - Ernst Ruska, Gerd Binnig, Heinrich Rohrer
- 1987 - J. Georg Bednorz, K. Alex Müller
- 1988 - Leon M. Lederman, Melvin Schwartz, Jack Steinberger
- 1989 - Norman F. Ramsey, Hans G. Dehmelt, Wolfgang Paul
- 1990 - Jerome I. Friedman, Henry W. Kendall, Richard E. Taylor
- 1991 - Pierre-Gilles de Gennes
- 1992 - Georges Charpak
- 1993 - Russell A. Hulse, Joseph H. Taylor Jr.
- 1994 - Bertram N. Brockhouse, Clifford G. Shull
- 1995 - Martin L. Perl, Frederick Reines
- 1996 - David M. Lee, Douglas D. Osheroff, Robert C. Richardson
- 1997 - Steven Chu, Claude Cohen-Tannoudji, William D. Phillips
- 1998 - Robert B. Laughlin, Horst L. Störmer, Daniel C. Tsui
- 1999 - Gerardus 't Hooft, Martinus J.G. Veltman
- 2000 - Zhores I. Alferov, Herbert Kroemer, Jack S. Kilby
- 2001 - Eric A. Cornell, Wolfgang Ketterle, Carl E. Wieman
- 2002 - Raymond Davis Jr., Masatoshi Koshiba, Riccardo Giacconi
- 2003 - Alexei A. Abrikosov, Vitaly L. Ginzburg, Anthony J. Leggett
- 2004 - David J. Gross, H. David Politzer, Frank Wilczek
- 2005 - Roy J. Glauber, John L. Hall, Theodor W. Hänsch
- 2006 - John C. Mather, George F. Smoot
- 2007 - Albert Fert, Peter Grünberg
- 2008 – *not awarded till the moment of publishing this issue*

ISSN 1813-2065

Organized by I.S.A.R.E.S.T.

INVITATION TO PARTICIPATE

WHAT IS ENERGY?

Energy is neither created nor destroyed. This is called the principle of Conservation of Energy. In other words, the amount of energy in the universe always remains the same. And when we use energy, like burning wood to generate light and heat, we don't use it up; we simply transform it from one form of potential energy (fuel) into other forms of kinetic energy (heat and light).
Almost all energy transformations involve the production of heat, which is considered the lowest form of energy, because it quickly dissipates into the surroundings and is normally unavailable for further use. So, although the total amount of energy remains the same, the amount of "useable" energy constantly decreases. However, don't worry too much about the decrease of useable energy; our Sun is scheduled to produce solar energy for many years to come, so taking this course will not be a waste of your time (or energy).

Energy is all around us. It heats our homes, powers our light bulbs and appliances, fuels our cars and provides for a variety of professional careers that deal with its many elements. It also comes in many forms such as heat, light, chemical, mechanical and electrical energy. And, according to physicists, energy can neither be created nor destroyed, only converted from one form to another. So why learn about energy? The answer is because energy, and the conversion of energy from one form to another, is fundamental to our modern living environment. By knowing the principles behind energy generation and conversion, you will come away with a knowledge base that can be applied to nearly every modern electrical, mechanical and chemical device that uses or produces power.

To introduce more about the alternative and renewable energy sources and techniques, I.S.A.R.E.S.T. invites you to attend the scientific lectures organized by I.S.A.R.E.S.T. You are requested to contact the secretary of the society and register your attendance. The lectures can be held earlier due to the registered requests.

To all they would like to submit seminars or scientific lectures during the third semester of the **I.S.A.R.E.S.T.** (October, November and December) in 2008, you are kindly requested to contact the secretary of the **I.S.A.R.E.S.T.** for date and presentation arrangements of the seminars or lectures. Please, do not hesitate to participate in our activities, this chance might be required by young scientists in our country, IRAQ, to develop and grow as well as introduce the professors and experts in field. You could find us on the post address, emails and mobile below:

Mailing Address:

P. O. Box 55259, Baghdad 12001, IRAQ

Emails:

irq_appl_phys@yahoo.com

editor_ijap@yahoo.co.uk

odayata2001@yahoo.com

Mobile:

00964-7901274190

Laser-Human Skin Interaction: Analytical Study and Optimization of Present Non-Ablative Laser Resurfacing

Walid K. Hamoudi

Nizwa University,
Birkat Al-Mouz,
P. O. Box 33,
Postal Code 616,
Nizwa, Oman
walid_khk@hotmail.com

There have been numerous of articles, reports and papers published on non-ablative laser resurfacing, showing the treatment of a wide range of tissue types, laser systems and doses and subject ages. Despite the fact that laser-skin interaction is affected when changing any of the laser parameters, many authors announced good results for the same skin conditions and disorders although different laser beam parameters were used. In their procedures they have adopted trial and error technique – a procedure that could cause some problems and side effects to patients. For random samples taken from the published articles [11-18] on non-ablative resurfacing, the authors used wide range of laser wavelengths (585-1320) nm, number of treatments (1-7) and fluences (2-179) J/cm^2. In addition, they used a very wide range of laser pulse durations (6ns-40ms) and some employed cooling while others did not. This article analyzes the results presented by some authors in order to define a better guide line for the use of lasers in this field.

Keywords: Laser-skin interaction, Laser resurfacing, Non-ablative treatment
Received: 21 July 2008, Revised: 21 August 2008, Accepted: 28 August 2008

1. Introduction

Human skin is the first line of defense against environmental effects. It is made of many thin sheets or layers of flat, stacked cells in which nerves, blood vessels, hair follicles, glands, and sensory receptors are found. It is constantly regenerated where cells created in the lower layer of the skin (dermis) migrate to the bottom of the upper layer (epidermis) [1]. Epidermis strongly absorbs ultraviolet (UV) radiation which causes sun tanned skin while near-infrared (NIR) penetrates deeply into the skin tissue. The relative effectiveness of optical radiation in penetrating the epidermis and dermis is proportional to cosine the angle of incidence. Collagen fibers are triple-helical amino acid compounds that are strengthened by cross-linking of prolene and hydroxyprolene.

There is an increasing interest in non-ablative skin resurfacing at a time where the ablative laser technique is declining due to the prolonged after-treatment medical care required. Non-ablative laser skin resurfacing creates a controlled injury to certain target structure in the dermis while completely sparing the epidermis from damage. This technique stimulates collagen generation and/or removes irregular pigmentation and enlarged vessels from the skin. Non-ablative technique can be employed either by heating the papillary dermal layer through the effect of water absorption spectrum or through the hemoglobin absorption of laser light with partial coagulation of papillary dermis [2].

Photo aging is the main factor of aging signs in which normal elastic fibers accumulate in an abnormal way while collagen fibers decrease in number and become disorganized. Non-ablative skin resurfacing is wavelength-dependent allowing different wavelengths to target different structures. Penetration is also wavelength-dependent which increases from several micrometers (um) in the UV to several millimeters (mm) in the infrared (IR). For non-targeted tissue, the laser pulse duration should be longer than its relaxation time, but to deliver all laser energy to the target tissue before it has a chance to cool down, the laser pulse duration must be shorter than the relaxation time of the target tissue [3].

Severe pain could be induced in human skin tissue when heated to a temperature of 45ºC; this corresponds to an injury threshold. When targeted tissue reaches ~60ºC, coagulation occurs. Laser light can exert its effect on selected tissue by thermal, mechanical and photochemical means. Mechanical effect of lasers on tissue-selective photothermolysis can target pigmented cells [2]. When a Q-switched (Q.S.) laser pulse is

used to treat pigmented tissue, a photo-acoustic shock wave is created, fragmenting the pigment into smaller particles i.e. loosing its coloring property. In the case of photochemical injury, a single photon has sufficient quantum energy to convert individual molecules to one or more different chemical molecules. The yield of the photochemical reaction products is proportional to the photon flux. Thermal energy depends on energy absorbed per unit volume (or mass) to produce a critical temperature elevation. Injury threshold depends on exposure time, the longer the length of exposure, the lower the temperature required to coagulate proteins and destroy tissue by elevated temperature.

2. Non-Ablative Laser Effects on Tissues

Skin resurfacing is one way to treat skin aging caused by many environmental, dynamic and gravitational effects. It allows gradual attenuation in the signs of skin aging [4]. Clinical signs of aging include the appearance of wrinkles, skin laxity, increased visible vascularity and pigmented spots. Improving skin texture is achieved by collagen remodeling. This is based on generating new fibers in the dermis to give the skin back its elasticity and can be triggered by heating the dermis and collagen fibers to a certain temperature.

Papillary dermal layer is heated due to the effect of water absorption of certain laser wavelengths (1200-2000) nm, but this requires many sessions. Laser light absorption by hemoglobin is another approach to change the skin metabolism [5]. This can help increase the blood supply to the targeted tissue resulting in microvasculature renewing, fibroblasts stimulation and new collagen production. Nd:YAG laser emitting at 1064nm has deep penetration (~4mm) with negligible absorption by the melanin and water, thus making micro-vascular hemoglobin the main target for fibroblast activation. Heat is generated in the papillary layer and spreads to the surrounding tissue. Epidermal temperature increases to 43-48ºC which means that the treatment doesn't require stringent anesthesia or cooling. An epidermal surface temperature of 40-48ºC is ideal since this correlates with dermal temperature of 55-65ºC that is needed for collagen re-modeling [6]. Laser pulse energy and duration are arranged for each patient to find the mildest mode for microvasculature treatment.

Non-ablative resurfacing induces a dermal healing response without notable injury to the epidermis. Improving the appearance of the skin is done by a sub-threshold laser-induced injury to the dermis and/or the dermal vasculature which results in a wound repair response and activation of the dermal fibroblasts. An inflammatory response within the dermis to the laser generated heat initiates a reaction that leads to collagen remodeling and an improvement in the appearance of the skin.

Cooling the skin surface during laser exposure is essential to protect the epidermis and superficial dermis from photo-thermal effects. Laser-heat induced injury to the dermis is then allowed without ablating the epidermal layer.

Laser beam interaction with material can introduce either thermal or wave effects but for dermatology, thermal effect is the dominant factor although wave aspects need more attention in this field. Not all lasers are useful to treat skin conditions or disorders, only those which have wavelengths that are absorbed efficiently in the targeted tissue are employed. It is not very clear to many users which laser is best for a specific case. Lasers can emit in a wide spectral range, and nowadays there are lasers emitting in the x-ray, ultraviolet, visible, NIR, mid infrared (MIR) and far infrared (FIR) spectra. Each laser is specified by its mode of operation (pulsed or continuous), output energy, duration & repetition frequency for the pulse types and average output power for the continuous types. Emitted wavelength or wavelengths in the case of the tunable lasers, line width which defines the temporal coherency of the beam, spatial content which shows the way the beam's energy is distributed, plane of oscillation or polarization of the beam and the beam spot size are other important aspects that have to be selected carefully. Based on the principles of selective absorption, the recommended lasers for non-ablative resurfacing are those of wavelengths absorbed by hemoglobin, water, melanin and pigments. Therefore dye lasers emitting at 532nm/585nm/595nm, semiconductor lasers emitting at 810nm/1450nm, Nd:YAG lasers emitting at 1064nm/1320nm and Er:Glass lasers emitting at 1540nm are preferred. Green 532nm and yellow 585nm and 595nm and to a lesser extent NIR 810nm laser are strongly absorbed by hemoglobin and melanin [7]. The heating effect in the dermis stimulates collagen remodeling and tightening. Non specific thermal injury initiates a wound repair response including fibroblasts activation and new collagen generation. The NIR 1064 nm has a very deep penetration into the skin and weak absorption by the melanin making it an ideal candidate for treating deep skin layers with little effect on the epidermal layer. For stronger absorption by water and much weaker absorption by melanin MIR 1330nm, 1450nm and 1540nm lasers perform better than the 1064nm.

3. Experimental Data for Non-Ablative Treatment

There are hundreds of articles cited in this field but a careful handling of the data presented will indicate that there is no clear rule or standard in selecting the laser parameters for treating certain skin disorder. Trial and error technique is adopted by many medical doctors which results in some pain and side effects to patients. In this section, a random selection of published articles on laser non-ablative resurfacing was made in order to show the "no standard" case in selecting the laser parameters.

One treatment of 5.516J/cm^2 and (6-20) ns laser pulses was used to treat rhytids but results showed different performance ranged from no improvement to good improvement [8]. Associated with mild edema and erythema, wrinkles were reduced [9] and skin texture was improved [10] when 10-20 J/cm^2, 3.2ms pulses of 1320nm Nd:YAG laser was used. Taking 7 treatments from 1064nm Nd:YAG laser, 34 patients were enrolled in a study to treat coarse wrinkles and skin laxity [11]. The author didn't put data for the laser he used, but reported an overall improvement of 40.6%. Using 2.4-3J/cm^2 and 350us pulses a 585nm dye laser was used to treat facial rhytids with a single treatment [12]. The author reported collagen increase by patients but no figure was given. Associated with mild blistering, two treatments of Nd:YAG laser operating at 1064nm with (120-179) J/cm^2 and (5-40) ms pulses was used, with contact cooling, to treat facial telangiectases [13]. Spider leg veins was treated using two treatments of (80-100) J/cm^2 and 60ms pulses from an 810nm diode laser [14]. The author reported a complete disappearance of the veins from some patients. Four treatments form 12000-14700 light pulses combined with 300µs, (7-9) J/cm^2 1064nm Nd:YAG laser were used without cooling to generate new collagen [15]. The author reported success for younger women only. Five treatments from a combination of 40J/cm^2 and 65ms 1064nm Nd:YAG laser and 9J/cm^2, 30ms of its frequency doubled 532nm lasers were used to treat skin rejuvenation [16]. The author reported 40% improvement in overall skin condition after four months. Scars randomly received three successive monthly treatments with a long pulsed 1320nm Nd:YAG laser on one facial half and a long pulsed 1450nm diode laser on the opposite facial half [17]. The results showed mild to moderate improvement with erythema, edema and hyper-pigmentation. A mono-therapy consisting of seven treatments of IPL and triple therapy consisting of seven treatments of IPL as well as nine treatments of low intense diode light and also bio-stimulation by drugs were tested. Improvement of 30% in skin texture and firmness with mono-therapy and 70% with triple therapy were achieved [18]. For treating blood vessels, one author stressed the need for a match between vessels thermal relaxation time and the laser pulse duration to avoid immediate purpura [19].

4. Analysis

Tracing every single article on non-ablative laser resurfacing is not an easy task**.** Unfortunately, a huge amount of data is not published in proper scientific journals; instead, they are presented in forms of internet pages, news, commercials and clinic reports. We want to present the subject from the scientific point of view and not on the trial and error method, which could lead to a misjudgment by low-skill medical doctors. We have to admit that what doctors are doing is a marvelous job by making thousands of people happy, by improving their appearances and ending their suffering from skin disorders. Better understanding to this subject is needed to optimize the results and make this application safer for everybody with no risk at all.

(500-1000)nm laser sources induce unwanted melanin absorption in the epidermis layer which could attenuate the laser intensity intended to target deeper tissue. By doing that, it will not leave the laser beam with sufficient heating power, especially in the treatment of dark skin or sunburn. Also, melanin absorption of these lasers can heat the epidermis and cause prolonged erythema and burn blistering. Too short nanosecond laser pulses means a very high peak power laser pulse that can destroy microvasculature instead of coagulating it. This is always accompanied by prolonged erythema. Long pulses (tens of milliseconds duration) are also not good for skin resurfacing since these widths exceed the time needed for micro vascular thermal relaxation.

Experimental data shown in section 3 indicate no clear standard adopted by medical doctors. Using a combination of more than wavelengths must be justified in advance and only for reasons based on the selective absorption principle, since every wavelength interacts with certain tissue. One can argue by saying why use a combination of 532nm and 1064nm on one side of the face and only 1064nm on the other side? Why for instance, not use the 532nm laser for the other side instead of the 1064nm? In another experiment thousands of ordinary light pulses were combined with the laser treatment, but why?

The experiments in the previous section show that for the same skin condition different lasers had been used, although a certain tissue interacts differently with different wavelengths. We can also see in table-1 that different repetition

 ISSN 1813-2065 Printed in IRAQ

frequencies (2 to 100Hz) and different pulse durations (6ns to $6.5x10^5$ns) were used for the same skin condition. Very short pulses produce very high laser peak powers, which can raise the temperature to a very high value and when it reaches 100ºC, the tissue vaporizes. This action will for sure give contradicting results. Repetition frequency is selected to cool non-targeted tissue between laser pulses and safe treatment by laser pulses is only ensured if the rules of selective absorption by tissues and confining of laser heat to this tissue are obeyed. The first requirement demands the correct selection of wavelength, while the second requires the right choice of pulse duration.

In addition to these two points, effective laser fluence and penetration depth into the tissue are very important. For pigmented targets (pigment cells, blood vessels), the laser pulse duration, τ ought to be equal to the relaxation time $\tau_{relax,}$ to allow good heat confinement and uniform heating of the target tissue. For collagen remodeling, on the other hand, thermal injury necessitates fast energy absorption in the tissue to obtain a large increase (10-25)ºC of tissue temperature for a short time. The selectivity of wavelength absorption occurs when the exposure time of the tissue to the laser light is shorter than the cooling time or thermal relaxation time. The energy dissipated to surrounding non-target tissue may cause collateral damage; the longer the relaxation time, the smaller the risk of coagulation necrosis to non-target structure. Once the relaxation time has elapsed, another laser pulse can be delivered to the targeted tissue without generating thermal damage to surrounding non-target tissue.

The experimental data above show the use of a wide range of laser energy fluences (2 to 179) J/cm^2. When tissue is heated to high energy fluence, a big rise in tissue's temperature will take place and consequently results can not be the same as those obtained with low fluences. Despite this, all authors of the experiments above announced good results. Using low laser fluence in order to avoid damaging the tissue must be linked with the fluence threshold required to initiate thermal injury and with the correct choice of laser wavelength to ensure the right absorption by the target tissue. Some data of section 3 above states that elderly people did not produce new collagen in response to the laser treatment while other data claimed collagen production by all patients, despite their different ages. Table (1) summarizes the data used for the experiments in section 3.

Table (1) Details of lasers used in non-ablative resurfacing

λ (nm)	F	τ	N	C	f (Hz)	Ass	Cond.	Ref
1064 Q.S. YAG	5.5	6-20ns	1	---	---	1, 30, 60, 90 days	Rhytids	11
1064 Q.S. YAG	2.5	6-20ns	1	---	---	4, 8, 14, 32 wks	Rhytids	8
1320 YAG	10	3.2ms	1 or 2	yes	100	---	Wrinkles	9
1320 YAG	10-30	3.2ms	---	---	---	---	Texture & tone	10
1064 YAG	---	---	7	---	---	1-6 wks	Wrinkles	11
585 Dye	2.4-3	350us	1	---	---	0-90 days	Rhytids	12
1064 YAG	120-179	5-40ms	2	yes	---	0-90 days	talengiectases	13
810 Diode	80-100	60ms	2	---	2-4	0, 2, 8, 52 wks	Spider vein	14
1064 YAG combined With light pulses	7-9	300µs	4	No	7	---	Collagen generation	15
Combination of 1064 YAG + 532 KTP + 1064 YAG	 40 24 9 ---	 65 30 30 ---	5(total) 2 2 2 3	---	2	1, 2, 6, 12 months	Skin rejuvenation Lower face (one side Periorbital of face) Opposite side of face Both sides of face	16
1320 YAG 1450 YAG			3			1, 2, 6, 12 months	Scars	17
IPL IPL + Intense diode Light + drugs	---	---	7 7 + 9 +drug	---	---		Hyper pigmentation Teleangectasias	18

λ: *laser wavelength (nm),* ***F:*** *energy fluence (J/cm^2),* ***τ:*** *pulse duration,* ***N:*** *no. of treatment,* ***C:*** *cooling,* ***f:*** *frequency,* ***Ass:*** *the follow-up assessment,* ***Cond:*** *the Skin condition and* ***Ref:*** *reference number*

At this point, it is useful to construct plots of absorption coefficients for both epidermis and dermis. The calculated values cover the range of all lasers used in non-ablative resurfacing. In epidermis, the estimated concentration of melanosomes per unit volume is expressed as the volume fraction of the epidermis occupied by melanosomes, see Table (2).

The above estimates are based on the wavelength dependence of the optical density of

epidermal melanin in the 650-800nm range and assuming a 60um epidermal thickness. The net epidermal absorption coefficient, $\mu a_{(epi)}$, combines both melanin and baseline skin absorption and is given as, [19]:

$$\mu a_{(epi)} = mel\% \times \mu a_{(mel)} + (1 - mel\%)\mu a_{(skin\ baseline)} \quad (1)$$

Table (2) Melanosomes per unit volume for adults [19]

Skin type	Melanosomes perunit volume (%)
light-skinned adults	1.3-6.3%
moderately pigmented adults	11-16%
darkly pigmented adults	18-43%

Table (3) lists the absorption coefficient values for epidermal layer due to skin baseline and melanin absorptions for a moderately pigmented adult with a 10% volume fraction of melanosomes.

Table (3) Absorption coefficients of epidermis for different laser wavelengths

λ (nm)	skin baseline μa (cm^{-1})	Melanin μa (cm^{-1})	epidermis μa (cm^{-1})
532	0.451	580	62.10
585	0.275	282	30.67
694	0.268	228	25.15
810	0.280	155	15.66
940	0.250	86	8 .74
1064	0.250	55	5.63
1320	0.250	38	3
1450	0.250	25	2
1540	0.250	20	1

Table (4) summarizes the absorption coefficient values of dermal layer due to the absorption of skin baseline, oxyhemoglobin and water. Figure (1) shows the absorption coefficient values of melanin, oxyhemoglobin and water as a function of the laser wavelength.

Table (4) Absorption coefficients of dermis for different laser wavelengths

λ (nm)	skin base μa (cm^{-1})	Oxyhemoglobin blood μa (cm^{-1})	Water μa (cm^{-1})	Dermis μa (cm^{-1}) x10^{-1}
532	0.45	400	0.0	84
585	0.28	150	0.0	33
694	0.27	1.5	0.0	2.9
810	0.28	5	0.0	3.7
940	0.25	7	0.0	3.8
1064	0.25	2,8	0.0	2.9
1320	0.25	0.0	1	7.8
1450	0.25	0.0	16	113
1540	0.25	0.0	10	78

The total optical absorption coefficient of the dermis, $\mu a_{(derm)}$ depends weakly on baseline skin absorption and strongly on hemoglobin and water absorption. The independent parameters of wavelength (nm) and volume fraction of blood (%) and water (%) can specify an average, $\mu a_{(derm)}$ in units of cm^{-1}. The baseline absorption of epidermis and dermis are sufficiently similar that can be treated by the parameter skin baseline μa. For a uniformly distributed blood and water in the skin, the net of dermis absorption coefficient is:

$$\mu a_{(derm)} = [blood\% \mu a_{(blood)} + water\% \mu a_{(water)} \quad (2)$$

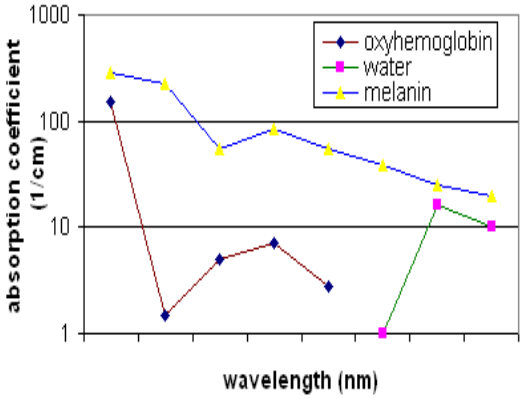

Fig. (1) Absorption coefficient of melanin, hemoglobin and water for some laser wavelengths

In Eq. (2), for a certain laser wavelength that have been chosen according to the principle of selective absorption, if the blood is the target, then all water parameters should be made zero. If on the other hand, the water is the target, then all blood parameters will be substituted by zero.

Up to 1100nm, the absorption coefficient of dermis is dominated by the absorption of blood, $\mu a_{(blood)}$, defined as having a 45% hematocrit. After 1100nm, the absorption coefficient of dermis is dominated by water absorption. Fig. (2) shows the absorption coefficient of epidermis and dermis as a function of wavelengths of interest after substituting in equations (1) and (2).

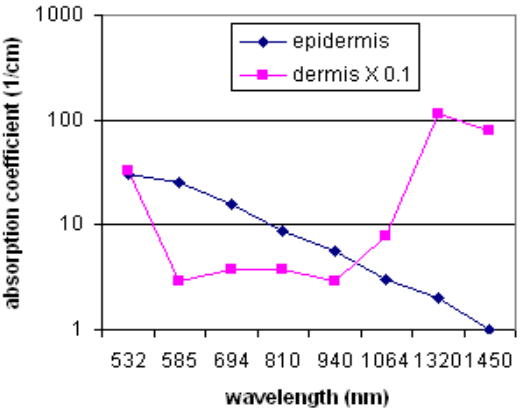

Fig. (2) Absorption coefficients versus laser wavelengths for epidermis and dermis

The average volume fraction of blood is 0.2%, however, for pigmented tissue as in port wine stain and spider veins, the volume fraction of blood is much higher than 0.2%. For such cases when assuming a 2% volume fraction of blood and using a 532nm laser, the absorption coefficient of dermis will be $8.4cm^{-1}$. A 70% of

water in the dermis will give values of dermis absorption coefficient shown in table (4) for some of the MIR wavelengths. The values of absorption coefficients of epidermis and dermis could be found different from one reference to another depending on the volume fraction of pigmentation, the value of average fraction of blood that had been assumed and the percentage of water content.

The rise in temperature (ΔT) of skin layer as a result of laser heating is [20]:

$$\Delta T = \left(\frac{ua}{\rho c}\right).F \qquad (3)$$

where ρ is the density, c is the specific heat and F is the laser energy fluence

The initial tissue temperature is then added to ΔT to find the final temperature. Table (1) shows a wide range of energy fluence used in the treatment. Putting these values in Eq. (3) will produce for the same skin condition temperatures that differ considerably from one experiment to another. The values of density (ρ) and specific heat (c) are 1.2g/cm^3 and 3.6J/g.°C for the epidermal layer and 1.2g/cm^3 and 3.8J/g°C for the dermis. It is extremely important to know what value of laser fluence and pulse duration should be used to certain skin conditions; otherwise, skin damage is inevitable. Improper choice of laser energy fluence could cause blistering and scarring to the patients instead of improving their skin appearances. Too short laser pulses heat the skin tissue very fast to a high temperature that could exceed the damage threshold whereas very long pulses cause gradual temperature rise which could not be enough to initiate certain effects. Let's substitute the value of the absorption coefficient for the dermis (8.4cm^{-1}) when 2% blood content is assumed using 532nm laser. Putting the value of fluence 9J/cm^2 used in reference -16, Eq. (3) will give a rise of temperature equal to 16.6°C. When this temperature rise is added to the initial temperature of the skin, 37°C, the final temperature will be 53.6°C. At this temperature the skin will be associated with inflammatory response. Following the same procedure, each value of fluence listed in Table (1) can be checked to know if the intended effect matches the skin's final condition. At 45-59°C, there is inflammatory response while at 60-80°C, there will be a skin death. When the temperature reaches 100°C, skin ulcer appears and if the temperature approaches 200°C the skin tissue will ablate.

To optimize the future experimental results, we need to consider the following:

(1) Threshold fluence to start thermal injury and maximum fluence, above which damage of tissue dominates, must be stated first to define the limits of laser energy fluence that can be used. This will, of course, be different according to tissue type, penetration depth, skin condition under treatment and absorption coefficient of the tissue for the laser wavelength used.

(2) Instead of energy fluence, we probably need to use a new parameter called thermal input density, measured in J/cm^3, which is the laser power density (W/cm^2) over irradiation speed (cm/s). Changing the speed for the same laser power and spot size will produce different temperature increases. High speed can raise the temperature of the skin by a small amount, while slow speed raises it to a high value. Using this new parameter will eliminate the effect of variable irradiation speed values.

(3) For certain Skin conditions, measuring technique and the assessment follow-up time need to be standardized in order to have proper evaluations and comparisons between results obtained by different doctors. All parameters listed in Table (1) should be considered as a standard routine to construct a clear picture of the procedure and the results.

(4) Doctors need to be aware of the term "depth of focus" especially in applications where a laser beam is needed to penetrate deep into the skin. This parameter is vital to decide the beam spot size at certain depth and consequently the temperature rise, especially when beam focusing is employed.

5. Conclusion

Trial and error technique in using lasers for non-ablative resurfacing is associated with some problems and discomfort to patients. Working out the required temperature and depth in advance can give better results for all skin conditions. At the same time, to have a better evaluation, standardization of treatment routine, measurements and assessment follow-up time is required. Knowing the values of the relevant laser parameters for certain skin conditions before treatment is vital to avoid skin damage. Instead of energy fluence, a new parameter called thermal input density is suggested to eliminate the effect of variable irradiation speed values.

References

[1] P. Talreja et al., *AAPS Pharm. Sci.*, 3(2) (2001) 1-9.

[2] R.Y. Ha, **"Lasers in plastic surgery"**, Selected reading in plastic surgery, 9, No. 40 (2003).

[3] **"Skin and Aging"**, ISSN: 1096-0120, Vol. 12, Issue (06) June (2004).

[4] M. Valeriani, *Lasers and Photonics*, Nov., No. 2, (2004) p.5.

[5] C. Hannapel, *Cosmetic Surgery Times*, 5, 4-02, May (2002).

[6] A. Alam et al., *Skin Therapy Letter*, Vol. 8, (2003).
[7] R.A. Weiss et al., *Dermatol. Surg.*, 25 (1999) 339-402.
[8] D.J. Goldberg et al., *Dermatol. Surg.*, Oct, 23(10) (1997) 903-906.
[9] J.S. Nelson et al., *Laser Surgical Med.*, 95 (1997) 32-33.
[10] G.M. Lipper, Conference report, American Society for laser Medicine and Surgery 2002: shedding light Medscape Dermatology 3(1) (2002).
[11] S.H. Dayan et al., *Arch. Facial Plast. Sur.*, 5(4) (2003) 310-315.
[12] Moody et al. *Dermal. Surg.*, 29:10 October (2003) 997-1000.
[13] D.M. Sarradet et al., *Dermatol. Surg.*, 29 (2003) 56-58.
[14] U. Wollina et al., *J. Cosmet Laser Ther.*, 5 (2003) 154-162.
[15] C.D. Schmults et al., *Arch. Dermatol.*, 140, Nov. (2004).
[16] M.-H. Tan et al., *Lasers in Surgery and Medicine*, (2004) 439-445.
[17] E.L. Tanzi et al., *Dermatol. Surg.*, 30(2) (2004) 152.
[18] T. Kono et al., *Annals of Plastic Surgery*, 59(5) (2007) 479-483.
[19] S.L. Jacques, **"Skin Optics"**, Oregon Medical Centre News. Jan. (1998).
[20] P. Mezzana, *Lasers in Medical Science*, 23 (2008) 149-154.
[21] S.L. Jacques et al., *Photochem. Photobiol.*, 53 (1991) 769-775.

This article was reviewed at Faculty of Health Science, University of Johannesburg, South Africa, and School of Applied Sciences, University of Technology, Baghdad, IRAQ

Recent Developments in Laser Cleaning

Written by
Martin Cooper
Los Alamos National Laboratory,
U.S. Department of Energy Laboratory,
California, U.S.A

Cleaning is a critical part of the conservation process. It serves not only to improve the aesthetic appeal of an object or building but also to reveal its true condition so that appropriate action can be taken to ensure that it survives for many future generations to enjoy.

During recent years there has been increasing concern over some of the more conventional methods of cleaning used on sculpture and sculptural decoration on historic buildings. Careless and inappropriate use of techniques, such as air-abrasive and steam cleaning, can lead to severe damage of the underlying stone surface. The loss of surface detail by overthorough cleaning can reduce the visual appeal of a surface and in extreme cases can even lead to its accelerated decay. Even if cleaning is carried out very carefully, techniques such as air-abrasive cleaning will result in some loss of material from a surface, particularly from a decayed crumbling surface, simply because abrasive particles cannot discriminate between the soiling and the stone surface. The removal of black encrustations from limestone sculpture is usually accompanied by removal of the patina which develops on the surface over a period of time and within which the original surface relief is preserved. Chemical-based cleaning techniques also have associated problems: chemicals often leave residues within the stone which can cause problems later on and once they have been applied their reaction cannot be suitably controlled. In Glasgow some sandstone buildings which were chemically-cleaned a few years ago are turning green at an alarming rate since ideal conditions for algae growth have been created on the surface. The development of laser-based techniques during the past few years has been a significant advance in making conservation methods less intrusive and more controllable. The fundamental difference between cleaning with laser radiation and conventional methods is that particles of light, or photons, can discriminate between the soiling and substrate. This allows the conservator to control the level to which the surface is cleaned.

The laser is a unique source of light, providing energy in the form of a very intense, monochromatic (a single colour or wavelength), well-collimated beam (a typical laser beam spreads out only a few millimetres after travelling several metres). When a laser beam interacts with a surface, part of the energy is reflected and the remainder is absorbed (assuming no transmission). The fraction of energy absorbed depends on the wavelength of the laser radiation and on the physical and chemical properties of the surface. A laser beam can have no effect on a surface unless it is at least partially absorbed.

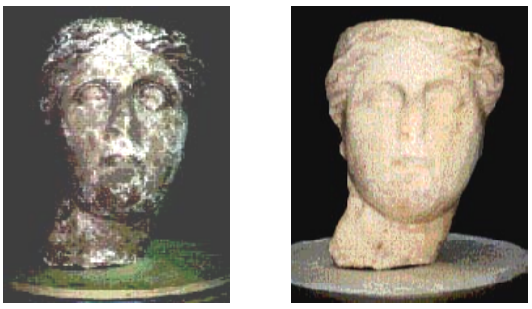

A Greco-Roman marble head excavated in Shropshire - left, after laser cleaning with an Nd:YAG laser - and far left, covered in soil and whitewash. The treatment removed all traces of soil and whitewash without damaging the marble surface

The most common laser used in conservation at the moment is the Q-switched Nd:YAG laser which provides short pulses (typically 5-10 ns long) of near infrared radiation at a wavelength of 1.064μm (or 1.064×10^{-6}m). These are effectively very short pulses of heat. The short pulse length is important since it prevents heat from being conducted beneath the soiling into the stone surface. This type of laser is commonly used since most soiling layers are much more strongly absorbing than the underlying substrate at 1.064μm. This means that, provided cleaning is carried out within safe parameters, once the dirt has been removed, further pulses will have no effect on the surface as insufficient energy is absorbed to cause any damage - in other words the process is self-limiting. The Nd:YAG laser is also

extremely reliable, easy to maintain, relatively compact and robust.

Commercial laser cleaning systems have become available during the last three years and are now being used by conservation studios across Europe. In a typical system the laser head, power and cooling supplies are housed in a single portable unit which weighs about 125kg and runs off a 13A/240V mains supply. In this case the laser beam is directed by means of a 7-jointed articulated arm with the beam emerging through a pen-like handpiece within which a lens is used to produce a diverging beam. The conservator controls the cleaning effect through adjustments to the energy in each pulse, the number of pulses fired per second (repetition rate) and the distance between the tool and the surface (which controls the intensity or spread of the beam). The maximum pulse energy and repetition rate varies between systems and a few systems use an optical fibre rather than an articulated arm to deliver the beam. Most commercial systems are suitable for work either in a studio or out onsite.

The most important cleaning parameter is the energy density, or fluence, of the laser beam which is defined as the energy per unit area incident on the surface (energy per pulse/beam size at the surface) and is usually measured in joules per square centimetre (J/cm^2). When working the fluence should be high enough to remove the dirt layers but low enough to ensure that the substrate surface is not damaged. At the Nd:YAG wavelength there is a safe 'working window' within which this can be achieved for a wide range of materials. This is the 'self-limiting' regime of laser cleaning. If the fluence must be raised above the damage threshold of the substrate in order to remove the soiling then the process will not be self-limiting and, as is the way with conventional cleaning methods, the conservator must attempt to stop the process as soon as the soiling has been removed to prevent any damage.

Laser cleaning occurs by a combination of mechanisms, the relative importance of each depending on the fluence used and the properties of the soiling. Since most types of soiling absorb strongly at 1.064μm, cleaning can usually be carried out at relatively low fluence (<1 J/cm^2) to minimise any risk of damage to the substrate. Strong absorption of energy leads to rapid heating and subsequent expansion of a dirt particle (see figure). Since the pulse length is so short the expansion happens so quickly that the resultant forces generated are sufficient to eject the particle from the surface. This is a very selective process. If the fluence is increased slightly then some material will be heated to a sufficiently high temperature to cause vaporisation. At higher fluences still (above approximately 1.5 J/cm^2; values depend on the properties of the soiling) the removal mechanisms become more complex and involve the formation of a plasma just above the surface and generation of a shock wave. This mechanism is less selective and can result in damage to the underlying substrate. Cleaning should therefore be carried out at the lowest practical fluence so that the more selective mechanisms operate.

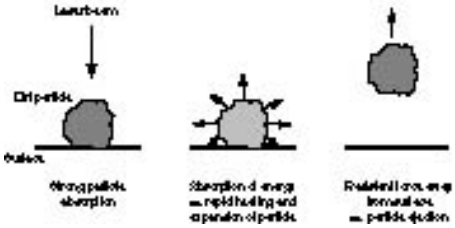

Schematic representation of dirt removal by 'rapid thermal expansion'. This selective mechanism appears to dominate the cleaning process at low fluence

Water can sometimes be used to enhance the cleaning effect. By brushing or spraying a thin coating of water onto the dirt surface immediately prior to irradiation, stubborn deposits of dirt can be removed without having to increase the fluence to unacceptably high levels. Dirt particles become coated with a thin film of water which is also able to penetrate into cracks and pores within the dirt layer. Absorption of the laser beam by the dirt layer occurs as normal and rapid heating at the dirt/water interface leads to explosive vaporisation of the water molecules, which exerts forces on and within the dirt layer sufficient to eject further material from the surface. The addition of water usually increases the cleaning rate significantly.

The main advantages of laser cleaning are:

Selectivity

Provided cleaning is carried out within suitable parameters it is possible to remove layers of dirt without removing any original material from the surface of the object. Such control allows the conservator to select exactly what is removed from a surface and also allows him or her to go back over an area which has already been cleaned to remove remnants of dirt without over-cleaning. The technique is sensitive enough to preserve the surface relief; original tool markings can be uncovered and delicate patinas left intact.

Non-contact

Since energy is delivered in the form of light there is no mechanical contact with the surface. This allows extremely fragile surfaces to be worked on.

Localised action

The laser cleans only where directed. A single laser can supply a beam with a diameter variable between a fraction of a millimetre and one centimetre, allowing the same tool to be used for both extremely precise and relatively large-scale work.

ISSN 1813-2065

Immediate control and feedback
The cleaning action is instantly halted once the laser is switched off so the conservator can stop the process whenever he or she decides. The condition of the surface can be continuously monitored by the conservator during cleaning, allowing decisions to be made at the earliest possible stage.

Environmental
Laser cleaning generates very small quantities of waste material (of the order 100g/m^2 for a uniform black soiling approximately 0.1 mm thick on outdoor limestone). The only waste generated is the dirt ejected from the surface which is straightforward to collect and dispose of using efficient extraction systems. There is no use of hazardous chemicals or solvents and the only protective clothing necessary is safety spectacles and a face mask. Laser cleaning is a clean and quiet technique which causes minimum disruption.

Versatility and reliability
Laser radiation at 1.06μm has successfully been used to remove dirt and other coatings from a wide range of materials including: marble, limestones, sandstones, terracotta, alabaster, plaster, aluminium, bone, ivory and vellum. In some cases the availability of radiation at other wavelengths can increase the flexibility of the tool, for example in the removal of some types of organic growth. As lasers have very few moving parts, they are also extremely reliable.
The laser described in this article has been designed specifically for work on sculpture and sculptural detail on buildings. More powerful laser systems capable of cleaning approximately ten times faster are available and would be more suitable for larger scale cleaning.
Laser cleaning does not work on everything. The cleaning of polychrome sculpture poses problems since different pigments absorb different amounts of radiation, certain types being very sensitive. For example, a single low-energy pulse will be sufficient to turn vermilion from red to black. In cases where there is evidence of pigment on a stone surface cleaning is usually carried out in such a way that the area is not exposed to laser radiation, unless it is known to be stable at the fluence being used.
Although laser cleaning of sculpture is usually much quicker than cleaning by the more sensitive conventional techniques, the large scale laser-cleaning of buildings cannot, at the moment, compete in terms of speed with techniques such as grit-blasting. It does however leave the stone surface intact. The development of laser systems is so rapid that it might not be too long before large-scale laser cleaning systems become available.
The relatively high initial cost of purchasing a laser system is seen by some as a disadvantage. This should be set against the low cost of maintenance and the savings that are made on time taken to complete a job. Purchasing a laser cleaning system is a long term investment. In the short term it might make more sense to hire an appropriate system for a particular job. Training courses are available which will teach the conservator when and how to use a laser.
During the past three years interest in lasers for cleaning has increased rapidly culminating in LACONA I, the first international conference on Lasers for the Conservation of Artworks which was held in Crete in October 1995. The conference brought together scientists, engineers and conservators to discuss current work (which includes the use of many different types of laser) and future developments in this rapidly expanding field.

Further Reading
Asmus, JF, Seracini, M and Zetler, MJ, *Surface morphology of laser-cleaned stone,* Lithoclastia, 1 (1976) pp23-45.
Verges-Belmin, V, Pichot, C and Orial, G, *Elimination des croutes noires sur marbre et craie; a quel niveau arreter le nettoyage? Conservation of Stone and other Materials*, Thiel, MJ (ed), Proceedings of the International RILEM/UNESCO Congress, Paris 29 June - 1 July 1993 pp534-541.
Cooper, MI, Emmony, DC and Larson, JH, *Characterisation of laser cleaning of limestone, Optics and Laser Technology*, 27 (1) (1995) pp69-73.
Cooper, MI and Larson JH, *The use of laser cleaning to preserve patina on marble sculpture*, The Conservator, 20 (1996).
Wilson, J and Hawkes, JFB, *Optoelectronics: An Introduction*, Prentice-Hall International (1983) pp254-261.
Tam, AC, Leung, WP, Zapka, W and Ziemlich, W, *Laser-cleaning techniques for removal of surface particulates*, Journal of Applied Physics, 71 (7) (1992) pp3515-3523.

Synthesis of Silicon Nanowires by Selective Etching Process

Agnes T.S. Yee

School of Material and Mineral Resources Engineering, Universiti Sains Malaysia, Penang, Malaysia

In this paper, selective etching process is used to synthesize SiNWs. This method arises from electroless metal deposition on a silicon wafer through selective etching. The electroless plating technique has many advantages such as low temperature processing and simple process with non-expensive deposition facilities. A clean p-type silicon wafer was etched in an aqueous solution containing hydrofluoric acid (HF) and silver nitrate ($AgNO_3$) at 60ºC for 60 minutes. This aqueous solution was prepared by mixing both HF and $AgNO_3$ in a plastic beaker and was heated in hot water bath. Electroless silver deposition will take place on the surface of Si wafer and their growth mechanism are analyzed on the basis of a self assembled localized microscopic electrochemical cell model. The structure of SiNWs is observed by using field emission scanning electron microscope (FESEM). It has revealed the formation of SiNWs with diameter ranging from 40 nm to 200 nm with the length of about 20 μm. The unique features of SiNWs have made them potentially applicable in solar cell, chemical sensing devices and basic components for nanoelectronic and optoelectronic devices.

Keywords: Silicon nanowires, Etching process, Silicon structures, CVD, PCVD
Received: 12 June 2008, Revised: 2 August 2008, Accepted: 9 August 2008

1. Introduction

Silicon nanowires (SiNWs) are one-dimensional nanostructure which have better feature compared to other low dimensional systems. SiNWs have two quantum confined directions while still leaving one unconfined direction for electrical conduction. Therefore, SiNWs are best used in applications where electrical conduction takes place. The small diameter of these NWs causes them to exhibit significantly different optical, electrical, chemical and magnetic properties from their bulk 3D crystalline materials. Various methods had been successfully used to synthesize SiNWs such as Chemical Vapor Deposition (CVD), Plasma Enhanced CVD (PECVD), Laser-Ablation and Evaporation. However, these methods involve high cost, high temperature, complicated equipments and other rigorous condition. Nanotechnology is expected to have an impact on nearly every industry. The U.S. National Science Foundation has predicted that the global market for nanotechnologies will reach $1 trillion or more within 20 years [1]. Many researches had been done in nanomaterials, nanoelectronics, and bionanotechnology throughout the years. Various methods to synthesize nanomaterials such as nanoparticles, nanowires, nanotubes, nanocomposites and nanostructured had been actively employed. Nanodevices and nanoelectronics have applications in medical treatments and diagnostics, faster computers, and in sensors.

It is reported that, upon exposure to ammonia gas and water vapor, the electrical resistance of HF-etched SiNWs is lower at room temperature compared to non-etched SiNWs. This phenomenon serves as the basis for a new kind of sensor based on SiNWs. The sensor is made by a bundle of etched SiNWs and exhibits fast response, high sensitivity and reversibility [2]. SiNWs can also be used to make diagnostic tools that are based on nanotechnology. These sensor devices can detect diseases in a person and give result within minutes [3]. In addition, SiNWs had been reported to have application in photodetectors and solar cells due to their tunable feature size and large surface area to enhance infrared response [4].

SiNWs are one dimensional and its small diameter had caused them to exhibit unique properties such as good electronic, optical, chemical and magnetic properties and will be a promising candidate for applications in nanodevices compared to bulk 3D material. SiNWs have two quantum confined directions while still leaving one unconfined direction for electrical conduction and therefore it is very conductive.

Throughout the years many effort have been made to improve the synthesis of SiNWs and these includes thermal chemical vapor deposition using SiH_4 gas at 650ºC in a flow mixture of H_2

 ISSN 1813-2065

and N_2 [5]. Besides that, Plasma Enhanced CVD (PECVD), Laser-Ablation [6] and Evaporation method [7] had also been employed to synthesize SiNWs. However, these synthesis techniques are tedious and troublesome and had always involved high cost, high temperature, complicated equipments and other rigorous condition.

In this paper, a simpler and cheaper method had been employed. This method involved electroless metal-particle-assisted etching [8]. Electroless metal deposition in ionic metal (silver) HF solution is based on micro-electrochemical redox reaction in which both anodic and cathodic processes occur simultaneously at the silicon surface [9].

2. Experimental Procedure

The substrate used in my experiment was a 2" p-type, B-doped Si(100) wafer, (0.75-1.25) Ω.cm. The wafer was first cut into pieces with the size of 1 cm^2 with a diamond cutter. Then the silicon wafer was cleaned with RCA technique to cleanse the surface from grease and debris. To avoid the wafer from being very brittle after etching, scotch tape were stuck onto the bottom surface of the substrate to prevent the bottom surface from being etched during the etching process. A solution consisted of 5 mol/L HF and 0.01 $AgNO_3$ were prepared in a container. The container used was a plastic beaker and the solution was heated to 60ºC in water bath prepared by filling water in a tray and was placed on top the hotplate. Once the temperature reached 60ºC, the silicon wafer was then etched in this solution for 60 minutes and the temperature was maintained during this process. A plastic tweezer was used to hold the wafer during the etching process to avoid the wafer from drifting and floating in the solution. After the etching process the wafer was rinsed with deionized water and was then placed in a glass beaker containing deionized water and cleaned ultrasonically for 60 minutes to detach the thick silver film from wrapping the surface of wafer. Lastly the wafer was rinsed with deionized water again and was then blown dry in air before microstructural observation. The morphology and chemical composition of the sample were characterized with field emission scanning electron microscope (FESEM) and energy dispersive x-ray (EDX).

3. Results and Discussion

Figure (1) shows a cross-sectional SEM image of the etched silicon wafer. It can be seen that the silicon nanowires formed are perpendicular to the surface of the wafer. The etched depth is approximately 20µm and the diameter of the nanowires are in the range of 40-200nm.

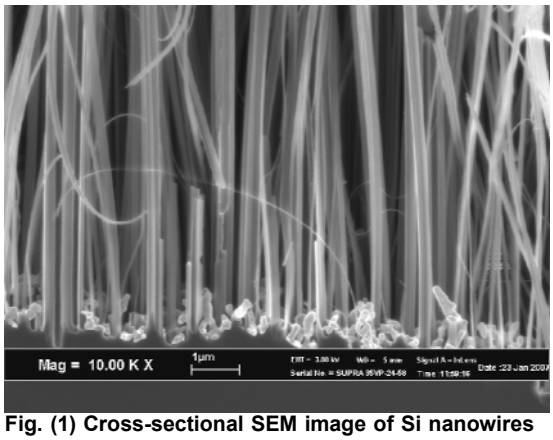

Fig. (1) Cross-sectional SEM image of Si nanowires with Ag sinking at the bottom

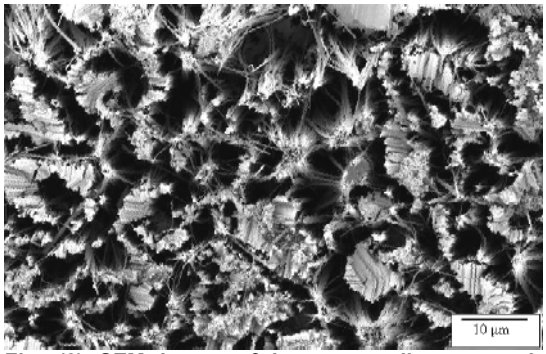

Fig. (2) SEM image of large-area silver capped SiNWs

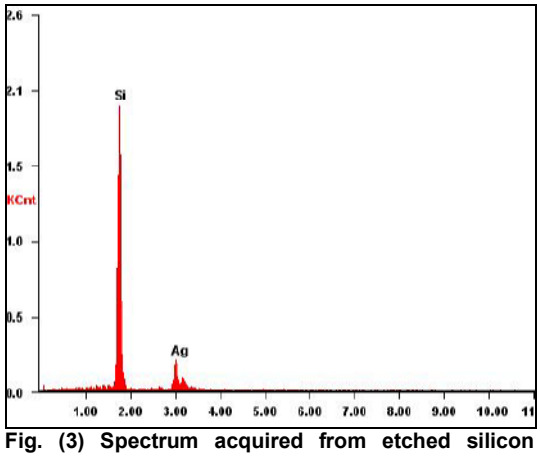

Fig. (3) Spectrum acquired from etched silicon wafer by EDX analysis

Figure (2) shows large area of SiNWs which have a cap-liked structure at the free end. The elemental composition was determined using EDX analysis. Fig. (3) shows the spectrum acquired from etched silicon wafer by EDX analysis. During the etching process, self-assembled localized microscopic electrochemical cell existed in silver nitrate HF solution. The silver deposition happened at the same time as the etching process at the surface of Si wafer took place. In the process of electroless metal

deposition, the silver nanocluster deposited on the surface of silicon wafer to form tree-like dendrites. The deposited silver atoms first form nuclei and then form nanoclusters which were uniformly distributed on the surface of the silicon wafer. The silver nanocluster and the Si area surrounding the silver nuclei acted as a local anodes and cathodes respectively. The electrochemical redox reaction process can be formulated as two half-cell reaction (1) and (2):

$$Ag^{+} + e^{-} \rightarrow Ag, \quad (1)$$

$$Si + 6F^{-} \rightarrow SiF_6^{2-} + 4e^{-}. \quad (2)$$

The silver nanocluster acted as a cathode was deposited and maintained at the surface of the wafer, while the surrounding silicon acting as the anodes is etched away. Therefore it was said that the nanoscale electrolytic cells leads to selective etching of silicon substrate. As the Ag catalyze the etching reaction, it then sunk below the surface and left behind columns of Si nanostructures with the length of approximately 20μm as shown in Fig. (4).

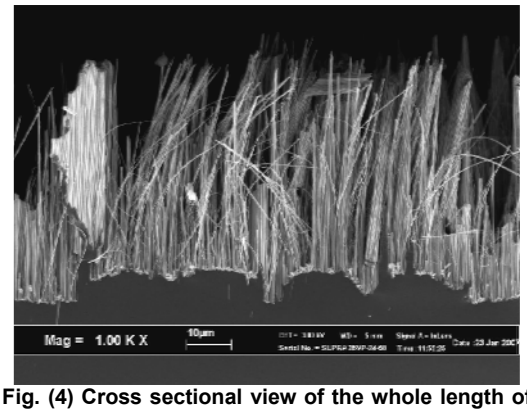

Fig. (4) Cross sectional view of the whole length of SiNWs

These nanowires can be used to make chemical sensors by adding two electrodes in between the bundled SiNWs and connecting dc source between the two electrodes. The gas molecules that pass through this sensor device will be adsorbed on the surface of the wires and thus changing the conductance of wires. This chemical sensor is something similar to what Zhou et al. [2] had proposed in their paper where they had produced SiNWs through oxide-assisted growth.

In addition, the etched silicon wafer does have structure similar to nanoporous. As reported in the work of Tucci et al. [10], these nanoporous can be used to fabricate heterostructure devices that show good responses to gas environment due to the interaction of absorbed gas molecules onto depleted porous silicon surface.

However, further studies are needed for utilizing this produced SiNWs as nanoporous to fabricate chemical or gas sensors. This is because the sensitivity of porous silicon depends on porosity, pore structure and size distribution of pores.

4. Conclusion

The selective etching process is an inexpensive and simple way to fabricate SiNWs. This technique is based on electroless metal-particle deposition, where self-assembled localized microscopic electrochemical cell existed in silver nitrate HF solution causing the silicon to be etched away. As a result, SiNW with the length of about 20μm and diameter ranging from 40-200nm were formed. These nanowires have promising characteristic that is useful for the nanoelectronic and optoelectronic devices.

References

[1] Nanotechnology Information Center, n.d, "What is the future of nanotechnology?", www.americanelements.com/nanotech.htm

[2] Zhou X.T. et al., *Chem. Phys. Lett.*, 369 (2003) 220-224.

[3] Parker R., "Nanowire Sensors to Provide Immediate Medical Test Results", Technical Proceedings of the Nanotechnology Conference and Trade Show, Vol.2 (2005) 119-122.

[4] Servati P. et al., "Silicon Nanowires for Photodetector Arrays", *Trends in Nanotechnology (TNT 06)*, Grenoble, France (2006) pp. 139-140.

[5] Yan X.Q. et al., *J. of Cryst. Growth*, 257 (2003) 69-74.

[6] Yu D.P. et al., *Solid State Commun.*, 105 (1997) 403-407.

[7] Fan S. et al., *Mater. Sci. and Eng.*: C, 15 (2001) 295-297.

[8] Kolasinski K.W., "Silicon Nanostructures from Electroless Electrochemical Etching", *Current Opinion in Solid State and Materials Science*, 9 (2005) 73-83.

[9] Qiu T. et al., *J. of Cryst. Growth*, 277 (2005) 143-148.

[10] Tucci M. et al., *J. of Non-Crystal. Solids*, 338-340 (2004) 776-779.

This article was reviewed at Institute of Material Science, National Academy of Science, UKRAINE and School of Applied Sciences, University of Technology, Baghdad, IRAQ

Coming

CONFERENCES & SYMPOSIA

Sponsored & Organized by Institute of Physics (IOP)

Advanced Measurement Techniques in Tribology
15 October 2008
Institute of Physics, London, UK
Organised by: the Tribology Group of the Institute of Physics

Sustainable Energy: New Solutions from Physics and Engineering
29 October 2008
Institute of Physics, London, UK
Organised by: the Applied Physics and Technology Division of the Institute of Physics

Preparation and Patterning of Magnetic Materials
4 November 2008
Institute of Physics, London, UK
Organised by: the Magnetism Group of the Institute of Physics

Experimental techniques in Semiconductor Research
19 November 2008
East Midlands Conference Centre, Nottingham, UK
Organised by : the Semiconductor Physics Group of the Institute of Physics

Low Temperature Techniques Course
26 November 2008
East Midlands Conference Centre, Nottingham, UK
Organised by : the Low Temperature Group of the Institute of Physics

BRSG Christmas Meeting 2008
10 December 2008
Institute of Physics, London, UK
Organised by : the BRSG Group of the Institute of Physics

Imaging to Understanding: Insight Through Visualisation
17 - 18 December 2008
Village Hotel, Nottingham, UK
Organised by: the Conferences Strategy Committee of the Institute of Physics

A Random Walk Through Polymer Science
19 December 2008
Institute of Physics, London, UK
Organised by : the Polymer Physics Group of the Institute of Physics

17th Interdisciplinary Surface Science Conference (ISSC 17)
30 March - 02 April 2009
University of Reading, Reading, UK
Organised by: the Thin Films and Surfaces Group of the Institute of Physics

Biological and Soft Matter
6 - 8 April 2009
University of Warwick, UK
Organised by: the Biological Physics, Liquids and Complex Fluids and Polymer Physics Groups of the Institute of Physics

Dielectrics 2009
15 - 17 April 2009
University of Reading, UK
Organised by: the Dielectrics Group of the Institute of Physics

Fourth International Conference on Conservation and Preservation Issues Related to Digital Printing
20 - 21 April 2009
Institute of Physics, London, UK
Organised by: the Printing and Graphics Science Group of the Institute of Physics

Influence of Deposition Parameters on Optical and Electrical Properties of Cu_xS Thin Films Prepared Using Chemical Bath Deposition Method

Ali M. Mousa [1*]
Samir H. Nasher [1]
Jean-Pierre Ponpon [2]

[1] *Material Research Unit, School of Applied Science, University of Technology, Baghdad, Iraq*
** alzyhery2000@yahoo.com*
[2] *InESS, Umr 7163, CNRS, Université Louis Pasteur, Strasbourg, France*

Thin films of Cu_xS have been deposited in an aqueous solution of copper chloride, tri ethanol amine, aqueous ammonia and thiourea. The effect of deposition time, solution pH and thiourea amount on films thickness, growth rate, optical and electrical properties has been studied. The film thickness increases with increasing deposition time and thiourea volume, whereas it decreases with increasing the solution pH. The corresponding small modifications of optical properties can be explained by the increase in roughness with film thickness. Electrical resistivity is strongly influenced by the solution pH and by the thiourea amount but depends to a much less extent on the film thickness.

Keywords: Cu_xS, Chemical bath deposition, Optical properties, Electrical properties
Received: 28 April 2008, Revised: 17 August 2008, Accepted: 24 August 2008

1. Introduction

Cu_xS exists in many different phases depending on the ratio of Cu in the compound, but the most important phase is the chalcocite with x=2. The material has a direct band gap of 2.26eV and an indirect gap of about 1.15eV and presents acceptor conductivity. Copper sulfide Cu_2S is a highly photoconductive wide band gap semiconductor and has been considered as an attractive material for solar cells, especially in association with CdS, giving efficiency close to 10% [1]. Cu_2S has also been used with polycrystalline conductive polymer [2].

Cu_2S thin polycrystalline layers have been deposited using many different techniques [3]. Among these Chemical Bath Deposition (CBD) is the cheapest one. It allows one to control the deposition process on different substrates with good stoichiometry [4-7]. The basic principle for CBD of Cu_xS requires the presence of both constituent ions i.e. Cu^{2+} and S^{2-}. The sulfide ions can be produced by the hydrolysis of the thiourea in a basic medium with pH=10-12 or in aqueous NH_3 [8], while the copper ions can be supplied by dissolved copper salts like ($CuCl_2.2H_2O$) [9-11]. When the copper salt is dissolved it gives first $Cu(H_2O)^{+2}$ and the formation of a complex follows. In the case of using NH_3 instantaneous transformation takes place: $Cu(NH_3)(H_2O)_5$ is transformed to the compound $Cu(NH_3)_4(H_2O)^{2+}$. In most published works Cu_xS is deposited from a solution of NH_3, $(NH_2)_2SC$ and $(CH_2CH_2OH)_3N$, where complex ions of $\{Cu(TEA)_n\}^{2+}$ or $\{Cu(NH_3)_m\}^{2+}$ and $\{Cu_4(TU_6\}^{4+}$ will be present, with relative concentrations changing with time of deposition process. The deposition of Cu_xS takes place when the ionic production of Cu^{+2} and S^{-2} is greater than the dissolving rate of Cu_xS.

In this work, we have studied the effect of the deposition parameters (deposition duration, thiourea amount, solution pH) on the optical and electrical properties of Cu_xS thin films prepared by CBD and determined by the values of deposition rates.

2. Experiment

The samples studied in this work were thin polycrystalline films of Cu_xS deposited by CBD on glass substrates with dimensions of 1x26x76 mm^3. Prior to deposition, the substrates were washed with distilled water in ultrasonic bath and then immersed for 24 hours in chromic acid (1gm of CrO_3 in 20ml of distilled water) and finally washed again with distilled water.

The total volume of the deposition bath was 50ml and made from 10ml of the following constituents:

1: $CuCl_2.2H_2O$ (0.5 mol/L);
2: TEA $(CH_2CH_2OH)_3N$ (9.4 mol/L);
3: NH_3 (30%);
4: Thiourea $(NH_2)_2CS$ (1 mol/L);
5: Double distilled water.

For a few experiments the volume of thiourea was adjusted between 5ml and 20ml. The volume of distilled water was modified consequently to maintain a constant 50ml total volume. All depositions were carried out at 30°C. The pH was adjusted between 9 and 13. The substrates were immersed vertically in the bath for times up to 4 hours. After deposition the samples were washed in distilled water and left to dry.

The crystallographic properties of the deposited films were determined by the X-ray diffraction technique using Cu-Kα radiation and scanning 2Θ in the range 10°-60°.

For optical measurements one side of the substrates was cleaned by using H_2SO_4 to remove the deposited layer. Thickness measurement was done by optical method using He-Ne laser light at an incident angle of 45°. The film thickness (t) was calculated using [12]:

$$t = \frac{\lambda}{2} \cdot \frac{\Delta x}{x} \quad (1)$$

where Δx is the width of the dark fringes and x is the width of light fringes

Optical transmission and absorption measurements were performed at room temperate in the 400-900nm range using a Lambda-9 Perkin-Elmer UV/Visible/NIR spectrophotometer. Values of the energy gap (E_g) were calculated from the extrapolated intercept of $(\alpha h\upsilon)^2$ versus $h\upsilon$, and absorption coefficient was calculated from transmission spectra using Beer-Lamberts law:

$$\alpha = 2.303 \frac{A}{t} \quad (2)$$

where A is the absorbance

The Reflectance (R) has been found by using the relationship

$$R+T+A = 1 \quad (3)$$

For electrical measurements two Aluminum electrodes in a coplanar configuration of 5mm width separated by 5mm were evaporated in vacuum on the surface of the deposited films. The Resitivity (R) was simply obtained by calculating the value of the dark resistance and using the relationship

$$R = \rho (L/A) \quad (4)$$

3. Results and discussion

As shown in Fig. (1) representing a typical X-ray diffraction spectrum with only a very broad peak, the prepared films are made of randomly distributed crystallites with amorphous phase. This result is in good agreement with previous results published on films prepared in the same way [6] and as deposited from acidic solution [13].

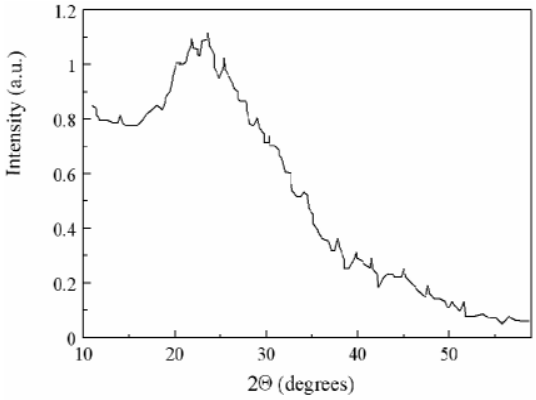

Fig. (1) Typical XRD spectrum of a Cu_xS film deposited by CBD

Fig. (2) depicts the film thickness variation as a function of deposition time, thiourea volume and pH value. Fig. (2a) shows that thickness increases linearly with the deposition time. The deposition rate is nearly constant and equal to 40.3nm per hour, such deposition rate is much greater than those obtained by chemical deposition [13], which need 8h to deposit a film of thickness (100nm) and no sign of saturation is noticed.

Fig. (2b) shows the dependence of the deposited film thickness on thiourea volume at a fixed deposition time (2hrs) and pH=11. Doubling the thiourea volume from 10ml to 20ml is accompanied by a thickness increase from 158nm to 233nm. Such an increment can be attributed to the increase in the number of S^2 in the thiourea volume which accelerates the reaction forming Cu_xS. Clearly, the deposition rate increases with the thiourea volume: it is 68.5nm/hour for 5ml, 79nm/hour for 10ml and becomes 117nm/hour for 20ml, while with using acidic bath the thickness increase quasi linear up to 0.3M and thickness of (200nm) and with more molarities saturation takes place. As shown in Fig. (2c), increasing the pH value at a fixed deposition time (2hrs) results in the thickness decrease. Although the effect on the deposition rate is smaller than in the two former cases, the influence of pH on the deposition rate is clear: starting with 87nm/hr at pH=9 it is only 62nm/hr at pH=13. Such a reduction can be due to the increase in the copper ions concentration (which is a function of the pH value).

Fig. (3) shows the spectral reflectance of four samples deposited for different times at constant pH and thiourea volume (pH=11, thiourea volume=10ml). For wavelengths shorter than 600nm the effect of deposition time is low. In contrast to higher wavelengths the reflectivity increases noticeably with increasing the deposition time. The same evolution can be observed for samples deposited at different pH values and different thiourea volumes. Although the influence of the increase of the number of

free carriers cannot be ruled out, it is more likely that this effect results from the increase in the film roughness with thickness.

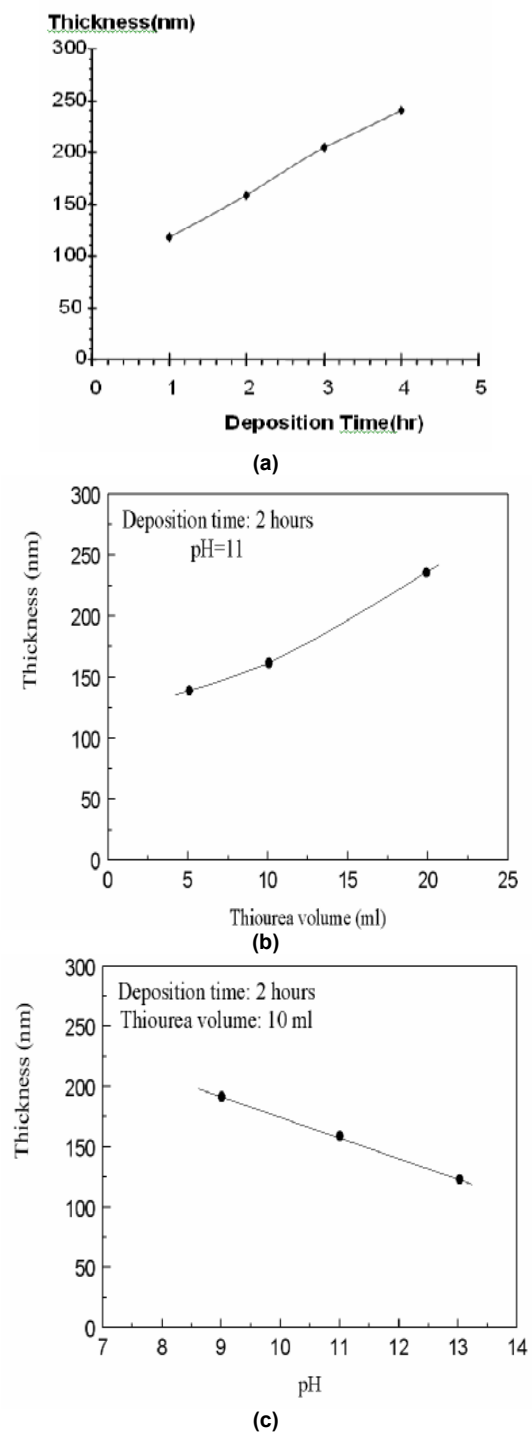

Fig. (2) Evolution of film thickness with (a) deposition time (b) thiourea volume (c) pH

The change in the absorption coefficient in the spectral range 400-900nm is depicted in Fig. (4) as a function of deposition time, thiourea volume and pH value, respectively. Only small differences appear depending on the experimental conditions. For wavelengths longer than 600nm these differences remain within the error limit. In the 400-600nm range, it follows by considering Fig. (2) that the thicker the film the lower the absorption coefficient.

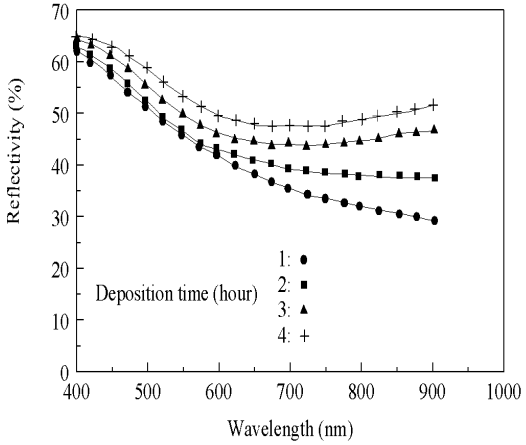

Fig. (3) Spectral dependence of the reflectivity with the deposition time (thiourea volume is 10ml, pH=11)

In any case the differences remain small. This result suggests the effect of some increase in film roughness with thickness actually the absorption coefficient is determined by the mean thickness of the film but the experimentally measured thickness is given by the maximum film height (which includes roughness). Therefore, according to relation 2 and assuming no change of the absorption coefficient throughout the whole thickness (due for example to a significant change in the film composition), overestimation of the film thickness used to calculate α leads to an underestimation of the absorption coefficient. This hypothesis is in agreement with the reflectivity behavior shown in Fig. (3). (Still it has to be remarked that a simple calculation shows that the optical effect of a significant roughness is equivalent to a change of the absorption coefficient in a more or less thin surface layer).

The band gap was calculated from the plot of $(\alpha h\upsilon)^2$ versus $(h\upsilon)$ Fig. (5) by using the values of the absorption coefficient. Except for the case of samples deposited for 1 hour (for which E_g=2.4eV), the value of the bandgap is 2.29eV, independent of the preparation conditions. These values differ from those obtained by chemical deposition with E_g=2.48eV for Cu_2S and 2.11eV for $Cu_{1.76}S$ [13].

ISSN 1813-2065

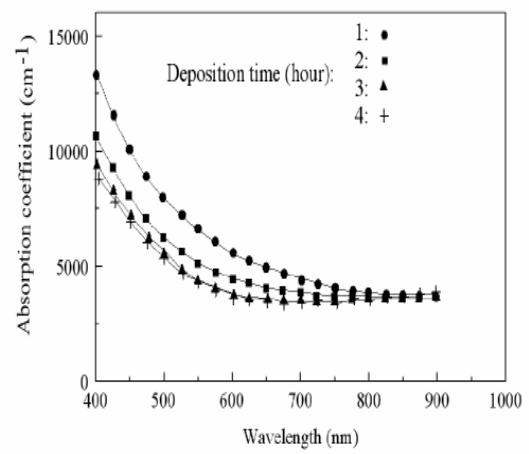

(a)

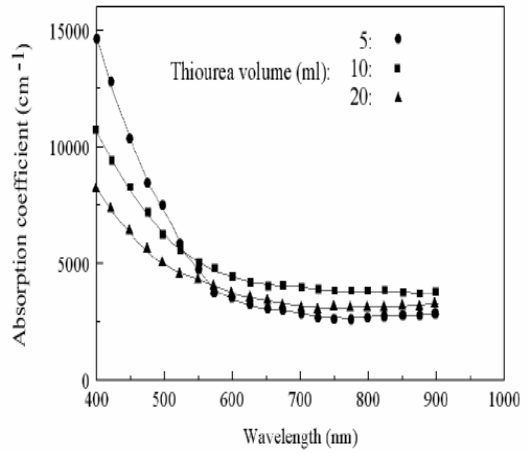

(b)

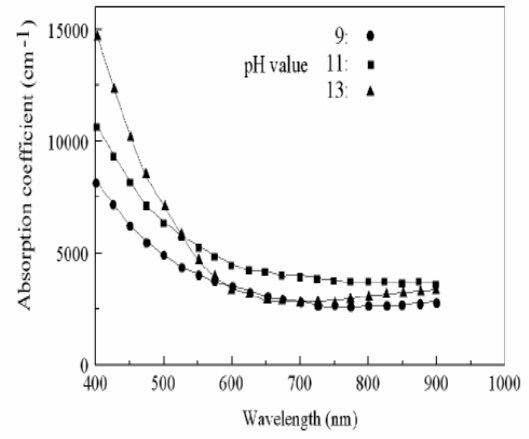

(c)

Fig. (4) Spectral dependence of the absorption coefficient with (a) deposition time (b) Thiourea volume (c) pH

The indirect bandgap value is not affected by the deposition time. Its value is 1.16eV for 10ml thiourea and pH=11. Increasing the thiourea volume decreases the indirect bandgap value (1.1eV for 20ml). On the other hand, increasing the pH increases the indirect bandgap (1.6eV for pH=13).

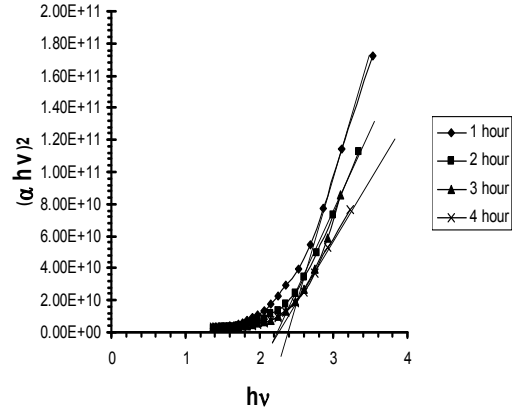

(a)

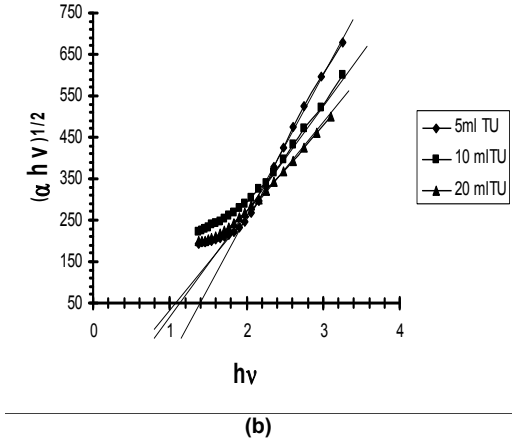

(b)

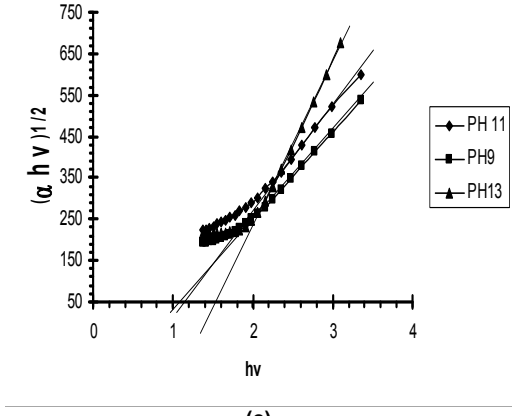

(c)

Fig. (5) The plot of $(ahu)^2$ versus (hu) for different deposition conditions (a) deposition time (b) Thiourea volume (c) pH

Fig. (6) shows the variation in the electrical resistivity as a function of deposition conditions. For pH=11 and thiourea volume=10ml, the resistivity is almost independent of the deposition time up to 3 hours (Fig. 6a). This result is consistent with former results obtained for films deposited by CD [14] but, as already reported, is in sharp contrast with the resistivity increase as a function of deposition time of evaporated Cu_xS thin films [15]. For 4hrs deposition time the resistivity decreases by a factor of two or three. As shown in Fig. (6b), increasing the thiourea volume produces copper

sulfide films which reach a very low resistivity (<0.03Ω.cm). In contrast, increasing the pH leads to a nearly exponential increase of the film resistivity (Fig. 6c).

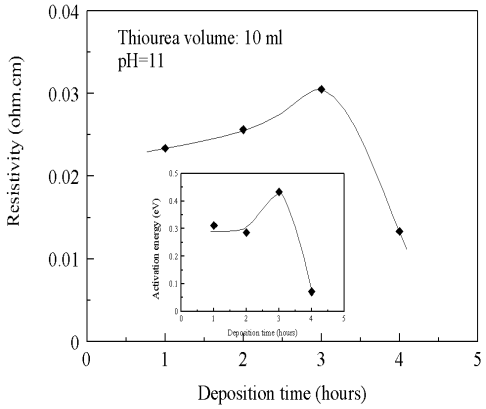

(a)

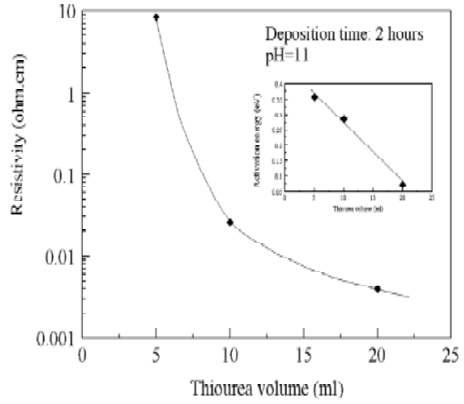

(b)

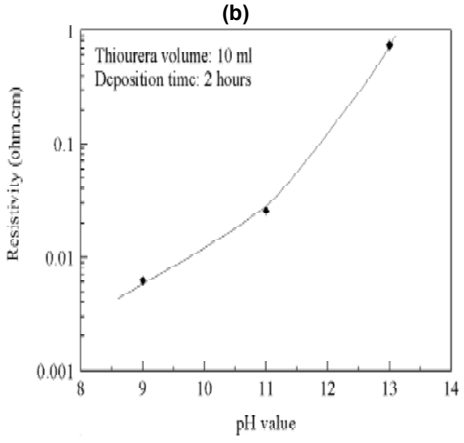

(c)

Fig. (6) Change in resistivity as a function of (a) deposition time (the insert shows the variation of activation energy of conductivity) (b) Change in resistivity as a function of thiourea volume (the insert shows the variation in activation energy of conductivity) (c) Change in resistivity as a function of pH

Determination of the activation energy of conductivity at different deposition conditions Table (1) by measuring the variation in the current I as a function of temperature T and plotting ln(I) *vs.* (1/T) as shown in Fig. (7), allows one to explain most of the previous results by considering an increase in the concentration of acceptor copper vacancies when increasing either thiourea volume or deposition duration. The insert of figure 5b for example shows the variation in the activation energy with thiourea volume for pH=11 and 2 hours deposition time. For the larger thiourea volume, the activation energy tends to go towards 0.07eV, which corresponds to the energy of the V_{Cu} level. The same holds for the influence of deposition time: up to 3hrs, the change in activation energy is low (0.3-0.4eV), insert of Fig. (6a).

Table (1) shows the values of activation energy as a function of deposition conditions

Sample	t_{dep} (hr)	pH	$V_{thiourea}$ (ml)	R (Ω.cm) x10^{-3}	E_a (ev)
1	1	11	10	23.387	0.312
2	2	11	10	25.6313	0.286
3	3	11	10	30.5347	0.433
4	4	11	10	13.3317	0.0712
5	2	11	5	8405.4	0.357
6	2	11	20	3.967	0.0723
7	2	9	10	6.18	0.099
8	2	13	10	737.8	0.078

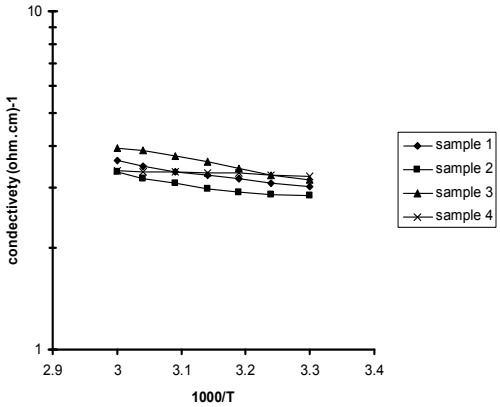

Fig. (7) The conductivity vs. temperature for 4 different samples

However, for 4hrs, the activation energy falls down to 0.07eV. Therefore, one can suppose that the resistivity decrease which is observed for long deposition time and large thiourea volume is induced by the creation of excess copper vacancies which give rise to a large number of free holes. Actually, as thiourea is the source for sulphur, one can expect a larger concentration of copper vacancies (equivalent to a stoichiometry deviation) with increasing the amount of thiourea. On the other hand, the large increase in resistivity with pH can be attributed to a deviation from stoichiometry due to the enhancement of the concentration of copper ions (related to the pH value, as already noticed).

4. Conclusion

Cu_xS films of a few hundreds of nanometer thickness have been prepared by chemical bath deposition for 1 to 4 hours. The film thickness increases with increasing deposition time and thiourea volume while it decreases with increasing the pH. Spectral reflectivity and absorption coefficient slightly depend on the film thickness probably due to an increase in the film roughness. Deposition time has a limited effect on electrical resistivity. In contrast, the pH value and thiourea volume have a large influence on resistivity and activation energy of conductivity.

References

[1] M.T.S. Nair and P.K. Nair, *Semicond. Sci. Technol.*, 13 (1998) 1164.

[2] M.C. Brelle et al., *Pure Appl. Chem.*, 72 (2000) 101.

[3] L. Isac et al., *Thin Solid Films*, 515 (2007) 5755.

[4] G.A. Alozie and F.C. Eze, *Globe J. Pure Appl. Sci.*, 9 (2003) 591.

[5] F.I. Ezema and P.E. Ugwuoke, *The Pacific J. Sci. Technol.*, 5 (2003) 33.

[6] J.G. Vazquez-Luna, A. Zehe and O. Zelaya-Angel, *Cryst. Res. Technol.*, 34 (1999) 949.

[7] I. Grozdanov, *Semicond. Sci. Technol.*, 9 (1994) 1234.

[8] P.K. Nair and M.T.S. Nair, *Solar Cells*, 22 (1987) 103.

[9] G.K. Padam and S.U.M. Rao, *Solar Energy Mater.*, 13 (1986) 297.

[10] G.K. Padam and Su. M. Rao, *Solar Energy Mater.*, 15 (1987) 227.

[11] D .Cahen, *Solar Energy Mater.*, 15 (1987) 225.

[12] K.L. Chopra, **"Thin Film Phenomena"**, McGraw-Hill Book Company.

[13] S.V. Bagul, S.D. Chavhan and R. Sharma, *J. Phys. Chem. Solids*, 68 (2007) 1623.

[14] H.M. Pathan, J.D. Desai and C.D. Lokhande, *Appl. Surf. Sci.*, 202 (2002) 47.

[15] B. Rezig, S. Duchemin and F. Guastavino, *Solar Energy Mater.*, 2 (1979) 53.

This article was reviewed at College of Materials Science and Engineering, Beijing University of Technology, CHINA, Department of Physics, University of Warsaw, POLAND, and School of Applied Sciences, University of Technology, Baghdad, IRAQ

Recent Developments in High Energy-Density Plasma Physics

Written by
Michael S. Murillo
Jon Weisheit
Los Alamos National Laboratory,
U.S. Department of Energy Laboratory,
California, U.S.A

High energy-density physics (HEDP) is one of the five technical pillars of the Stockpile Stewardship Program, and it is now recognized as an important, multidisciplinary area of research to be emphasized at the national level [1]. Conventionally, HEDP is defined as the study of matter under extreme pressures, in excess of one megabar. As Fig. (1) notes, HEDP science also is relevant to astrophysics and fusion energy research.

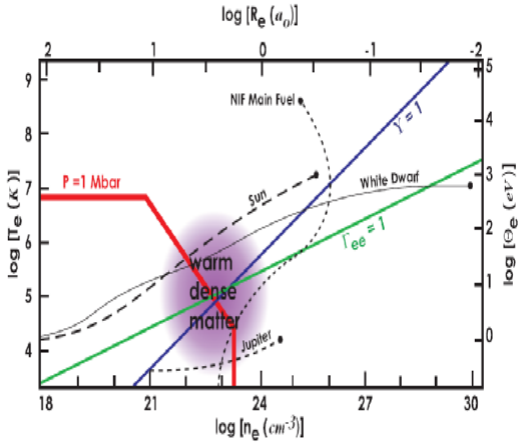

Fig. (1) The HEDP regime in the temperature-density plane. Above and to the right of the dark red line, the pressure of matter plus radiation exceeds 1 Mbar. Plasmas below the line Γ_{ee}=1 are strongly coupled, and those below the line Y_e=1 are degenerate. The tracks shown mark conditions within the Sun, Jupiter, a white dwarf star, and an imploding ICF capsule

A plasma's ionic charge states, and the many-body correlations among its particles, influence its equation of state, its transport coefficients, and its radiation spectrum, so it is useful to illustrate HEDP effects on these basic quantities. Fig. (2) reveals that even a "simple" issue like ionization balance can be difficult to treat accurately in dense plasmas: the Saha equation (appropriate at low densities) predicts mean charge states <Z> that differ substantially from the values of <Z> predicted by the Thomas-Fermi equation (appropriate at high densities). Moreover, both of these prescriptions incorporate simplifying assumptions that, at best, are questionable under HEDP conditions, and neither is valid for nonequilibrium plasmas. Further, the Saha equation yields charge state fractions – essential for spectroscopy – but the Thomas-Fermi equation yields just <Z>.

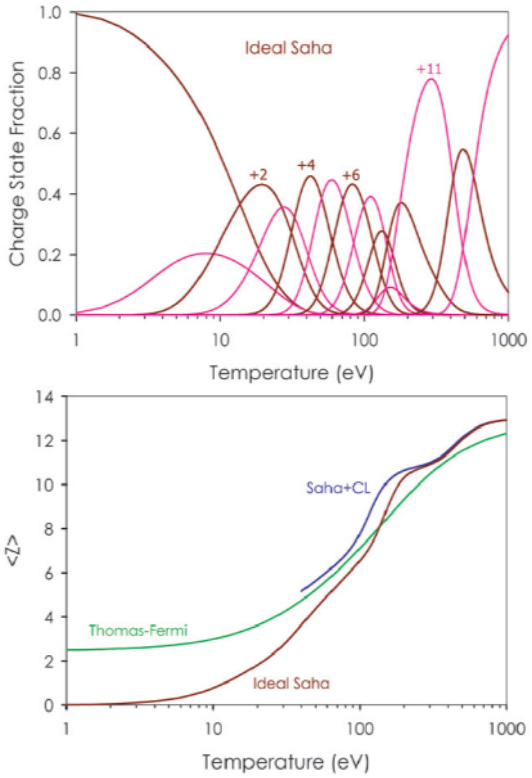

Fig. (2) The variation of mean charge state <Z> with temperature in an aluminum plasma at solid density (2.70g/cm^3), as predicted by the Saha and Thomas-Fermi equations (lower panel. Corresponding Saha charge state fractions (upper panel)

ISSN 1813-2065

A second example of HEDP effects is shown in Fig. (3), which plots radial distribution functions $g(r)=n_i(r)/n_i$ in a one component plasma of ions (charge Ze) embedded in a uniform density background of electrons ($n_e=Zn_i$), for different values of the Coulomb coupling parameter $\Gamma=(Ze)^2/a\Theta$, where Θ is the temperature in energy units and $a=(3/4\pi n_i)^{1/3}$ is the mean inter-ion spacing. Radial distribution functions for the larger Γ-values exhibit peaks that indicate substantial short-range order in the plasma.

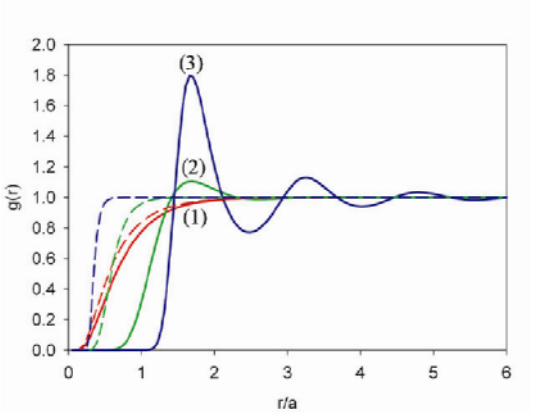

Fig. (3) Radial distribution functions g(r), which measure the expected density of ions neighboring one at the origin, are plotted versus scaled distance r/a, for (1) Γ=1 (red), (2) Γ=10 (green), and (3) Γ=100 (blue). Solid lines: hypernetted-chain theory. Dashed lines: analytic model using Debye potential of mean force

Within the past year, we reviewed many of the concepts and methodologies (from hydrodynamics, condensed matter, statistical, plasma, and atomic physics) that underlie the field of HEDP [2, 3]. Novel ideas and experiments are needed to better understand and model matter that may be far from equilibrium, strongly coupled by Coulomb interactions, and/or involve degenerate electrons, so one goal of our work was to identify challenging problems in this subject that are important generally to the Nuclear Weapons Program and that could be tackled effectively with present Los Alamos National Laboratory capabilities.

Due to particular Theoretical (T) Division strengths and interests in theory and simulation, three important HEDP subjects have now been identified for emphasis: *Quantum simulation methods* (our essential enabling "technologies"—quantum Monte Carlo, quantum molecular dynamics, and wavepacket molecular dynamics); *Radiation Hydrodynamics* (equation of state for mixtures, opacities of inhomogeneous media, turbulence effects, astrophysical and fusion applications); and *Nonequilibrium Phenomena* (relaxation, particle transport, nuclear reactions, laser-plasma interactions, intense magnetic fields).

At last count, more than a dozen specific projects within these areas are already underway or are being organized. These T-Division efforts involve partnerships with both theoretical (e.g., Applied Physics and Computer and Computational Sciences) and experimental (e.g., Physics, Materials Science and Technology, and the Los Alamos Neutron Science Center) divisions at LANL, as well as external laboratories and universities.

References

[1] "Frontiers in High Energy Density Physics," National Research Council, 2003.

[2] M.S. Murillo, "Strongly Coupled Plasma Physics and High Energy-Density Matter," *Phys. Plasmas* 11, 2964 (2004).

[3] J. Weisheit and M.S. Murillo, "Atoms in Dense Plasmas," in *AIP Handbook of Atomic Molecular and Optical Physics,* 2nd ed. (Springer, New York, in press).

Jelena Ninković

Max-Planck-Institute for Physics, Föhringer Ring 6, Munich, Germany

Recent Developments in Silicon Photomultipliers

A novel type of avalanche photodetector with Geiger mode operation, known as a Silicon PhotoMultiplier (SiPM) provides an interesting advance in photodetection and is already an alternative to traditional PMTs in many applications. The state of the art of the silicon photomultipliers (SiPMs) - their main properties and problems - are discussed.

Keywords: Single photon counting; Silicon photomultiplier, BID SiPM
Received 10 May 2008, Accepted 15 July 2008

1. Introduction

Development of photodetectors for the detection of lowintensity photon flux is one of the critical issues for experimental physics, medical tomography and many other areas. In most of these applications as a photodetector standard PhotoMultiplier Tubes (PMTs) are used. However, PMTs have two main problems: they are very sensitive to the magnetic fields and command a high price due to the complicated production process. The search for an alternative detector started a long time ago. A promising candidate for the replacement of PMTs was the Avalanche PhotoDiode (APD). Although it has an internal gain it was not capable of detecting single photons. At the beginning of this millennium a new detector concept was developed, a silicon photodetector operated in limited Geiger mode, capable of detecting single photons like a PMT and was therefore given the name Silicon PhotoMultiplier (SiPM). For the past few years mainly Russian groups pursued the development of the new type of APD [1–3], but today the interest for these devices is increasing and they are being developed on many places around the world. Recently, a new concept was introduced: A Back Illuminated Drift Silicon Photomultiplier (BID SiPM) where an APD is combined with a drift diode to form a building block for photodetector arrays [4–6]. These devices are to be produces in Max-Planck-Institute Semiconductor Laboratory [7].

2. The Silicon Photomultiplier Concept

A silicon photomultiplier (SiPM) is an array of small APDs (cells) combined to form a macroscopic unit (typically 500 to 4000 cells per mm^2). Each cell operates in limited Geiger mode. A small polysilicon resistor, which connects the cell to a conductive grid, limits the current through the junction and quenches the avalanche once the cell capacitance has been discharged. Single cells produce a standard signal when any of them is brought to breakdown. In the silicon photomultiplier (SiPM) the independently operating APD cells are all connected to a common readout line. Therefore, the output signal is the superposition of the standardized signals from all fired cells. In the case of the BID SiPM concept radiation enters from the back of a fully depleted wafer and the photoelectrons are focused (drifted) onto a small ‘‘point-like’’ avalanche region located on the front side.

3. Properties of Silicon Photomultiplier

A silicon photomultiplier (SiPM) provides an intrinsic gain for single photoelectrons at the level of $\sim 10^6$. The amplitude of a single cell is proportional to the capacitance of the cell times the overvoltage (the difference between the operation voltage and the breakdown voltage). 1It should be noted that two photoelectrons detected by single cell are producing same output signal as a single one. Therefore, one cannot distinguish if one or more photoelectrons have been detected by a cell. In case of not too intense light flashes, the number of fired cells is in first order proportional to the number of photons thus compensating for the missing dynamic range of a single Geiger mode APD. For large light flashes saturation effects set in. In reality, the process is more complex because of the recovery time of the cells and the influence of dark current. The main domain of operation for silicon photomultipliers (SiPMs) is for light levels with a photoelectron flux $<<1$ photoelectron/cell/recovery time.

These devices have an excellent photon counting capability (see Fig. 1) which comes as a consequence of good cell to cell gain uniformity, negligible contribution of electronic noise and a very low excess noise factor of single cells. Unfortunately, the breakdown can be triggered not only by an incoming photon but also by any generation of free carriers. The latter produces dark counts at a rate from 100kHz to several MHz per mm^2 at 25°C and with a threshold at half of the one photon amplitude. Thermally

generated free carriers can be reduced by cooling. There is a factor 2 reduction of the dark counts every 8–10°C.

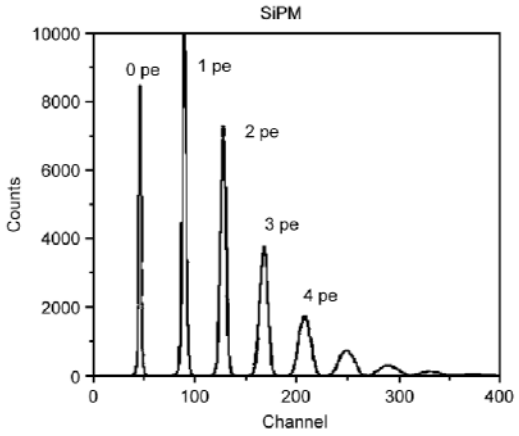

Fig. (1) Pulse height spectrum of light pulses with very low intensity recorded with a silicon photomultiplier (SiPM) [11]

Another possibility is to operate at lower bias resulting in a smaller electric field and thereby lower Geiger efficiency. Field-assisted generation (tunneling) can only be reduced by using a smaller electric field. The dark counts can also be reduced in the silicon photomultiplier (SiPM) production process by minimizing the number of generation-recombination centers, the impurities and crystal defects. The BID SiPM is expected to have an increased dark rate due to the bigger active volume. In order to keep dark rate lower one has to maintain good technology. Further reduction can be achieved by making the devices thinner.

In many applications the fact that in an avalanche breakdown there are in average three photons emitted per 105 carriers with a photon energy higher than 1.14eV [8–10] may be considered a disadvantage. When these photons travel to a neighboring cell they can trigger a breakdown there. This gives rise to optical crosstalk which violates the pixel independence and leads to a non-Poissonian behavior of the distribution of the number of fired pixels. It acts like shower fluctuations in an APD. It is a stochastic process and introduces an excess noise factor like in a normal APD or a PMT. The crosstalk can be reduced in a dedicated design with implementation of grooves between the cells, which act as an optical insulation. Since the concept of BID SiPM is based on point-like high-field regions the cross talk effect should be reduced. However, a final evaluation can be performed only after the first prototype production.

The timing properties of silicon photomultipliers (SiPMs), even for single photoelectrons, are excellent (a FWHM of 123ps has been measured for a single cell [11]) mainly because the avalanche breakdown process is fast and the signal amplitude is large. Fluctuations in the avalanche process are mainly due to a lateral spreading (~10ps) by diffusion and by the photons emitted in the avalanche [8]. Operation at high overvoltage (high gain) may slightly improve the time resolution. For the BID SiPMs drifting of photoelectrons increases the time jitter. Reduction of the pixel size improves time jitter but increases the cross talk.

The photon detection efficiency (PDE) of silicon photomultipliers (SiPMs) is to the first order the product of the quantum efficiency (QE) of the active area, a geometric factor (ratio of active to total area), the probability to initiate an avalanche breakdown (Geiger efficiency) and the fraction of active cells, i.e. those cells which are not quenched or are still recovering from a previous breakdown. Quantum efficiency (QE) is maximal 80–90% depending on the wavelength. It peaks in a relative narrow range of wavelengths because the sensitive layer of silicon is very thin. Devices with n-silicon on a p-substrate are more sensitive for green and red light and less for blue light because only the photons with longer wavelengths penetrate deep enough into the silicon (see Fig. 2). Additionally, electrons have a higher Geiger efficiency compared to holes.

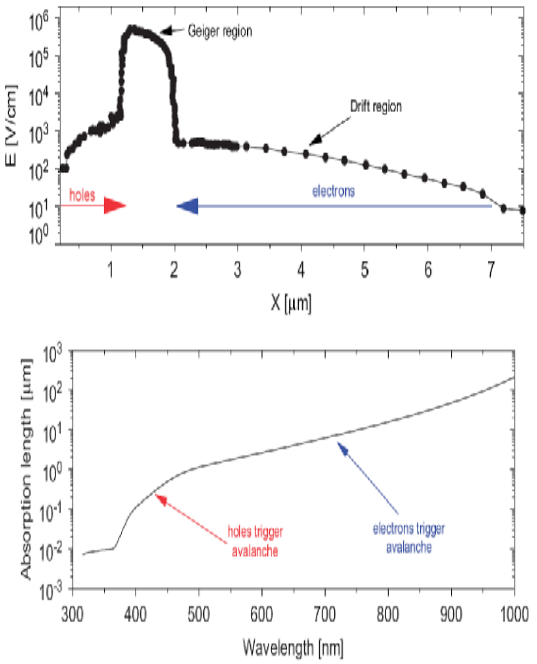

Fig. (2) Influence of difference in behavior of electrons and holes on the PDE. Top: electric field distribution in epitaxial layer (after Buzhan et al. [12]). Bottom: light absorption in silicon

The geometric factor, which is limited by the dead area around each cell, depends on the construction and ranges typically between 20% and 70% of the total area. This is the parameter that can be optimized for specific application.

Typical values of the PDE of recent silicon photomultipliers (SiPMs) [13] are comparable to the QE of conventional bialkali photomultipliers. The main advantage of the BID SiPM concept is its expected PDE. The geometrical fill factor of 100% as well as a non-structured radiation entrance window, that allows deposition of different antireflective coatings [6,14,15], make this device unique and superior compared to silicon photomultipliers (SiPMs). A PDE as high as 85% at 400nm can be expected for these devices [6].

4. Conclusions

Silicon photomultipliers (SiPMs) are already now an alternative to photomultipliers (PMTs). They are the better choice for the detection of light with very low intensity when there is a magnetic field and when space and power consumption are limited. Most of the devices are still small ($1x1mm^2$ ... $5x5mm^2$) but areas of $10x10mm^2$ are planned in the near future. The development started some 10 years ago but there is still a wide room for improvements. Many parameters can be adjusted to optimize the devices and to tailor them for special needs. However, one has to take into account that there are many cross-correlations which make it impossible to build a perfect device. Compromises are necessary and the device has to be optimized for its specific application. For example trenches reduce crosstalk, which allows the overvoltage increase improving the PDE and UV response but they still reduce the fill factor. For the use in PET, a high dark rate is uncritical, as one is interested in signals that exceed the one photoelectron level by a large margin while the integration window is only a few tens of nanoseconds for fast scintillators. For application in high-energy astrophysics devices with high PDE will increase the effective sensitivity of the experiment and therefore lower the observational threshold. Therefore the BID SiPM would be a better choice in this case.

References

[1] B. Dolgoshein, et al., *Nucl. Instr. and Meth.* A 504 (2003) 48.
[2] V. Golovin, Patent No. RU 2142175, 1998.
[3] Z. Sadygov, Patent No. RU 2102820, 1998.
[4] G. Lutz, et al., *IEEE Trans. Nucl. Sci.* NS-52 (2005) 1156.
[5] G. Lutz, et al., *Nucl. Instr. and Meth.* A 567 (2006) 129.
[6] J. Ninkovic, et al., *Nucl. Instr. and Meth.* A, 2007, doi:10.1016/j.nima.2007.06.060.
[7] MPI Halbleiterlabor,http://www.hll.mpg.de/i.
[8] A. Lacaita, et al., *IEEE Trans. Electron. Devices* ED-40 (3) (1993) 577.
[9] A. Lacaita, et al., Appl. Phys. Lett. 62 (1992).
[10] A. Lacaita, et al., *Appl. Phys. Lett.* 57 (1990).
[11] P. Buzhan, et al., *Nucl. Instr. Meth.* A 504 (2003) 48.
[12] P. Buzhan, B. Dolgoshein, et al., An advanced study of silicon photomultiplier, ICFA Instrumentation Bulletin, 2001.
[13] B. Dolgoshein, Proceedings from LIGHT2006, to appear.
[14] R. Hartmann, K. Stephan, L. Strueder, *Nucl. Instr. and Meth.* A 439 (2000) 216.
[15] R. Hartmann, et al., *Proc. SPIE*, 5903 (2005) N1.

This article was reviewed at School of Applied Sciences, University of Technology, Baghdad, IRAQ

Wide Band-Gap Compound Semiconductors for Solid State Device Development

Written by
Shahid Aslam
NASA Goddard Space Flight Center,
Code 685, Greenbelt, MD 20771
U.S.A

The challenge

Currently, researchers are working on more than 40 compound semiconductors many of which are wide-bandgap materials. Over the last nine years we have witnessed the emergence of a compound semiconductor industry that is distinct from the silicon semiconductor industry. Given this fact , and the obvious success of consensus-based planning in the silicon arena, we think that the time is ripe for us to put the emerging wide-band gap materials onto the NASA Advanced Planning and Integration Office strategic roadmap. It must be stressed that, the development of electronic devices does not happen in isolation from materials development. It is therefore crucial, in developing a strategic roadmap, to identify those material systems that will give rise to the next generation of low-noise devices and detectors for NASA directed missions. With this in mind we have to forge links and partnerships with those institutions (commercial and academic) that have a stake in this development, so that we can maintain R&D costs to a minimum. Compound semiconductors were initially driven by defense funding and even today tend to require more fundamental research from university, industry and government laboratories like our-selves. In part, this is because the materials base is very broad and engineering process' within each materials system is not consistent. A wide plethora of problems have been identified where topics include compatible substrates; p-type doping issues in (Al,In)GaN and Zn(Mg)O, device physics and fundamental defect densities. We need to find alternatives to sapphire and SiC as substrates such as lithium gallate, silicon (for development of on-board intelligence and for development of multi-colour sensors) and free standing GaN quasi-substrates produced by laser lift-off. Other challenges are the need for 4 inch and greater wafer growth technology to accommodate large format array (>1Kx1K) development. We need to work on nitride HEMTs and SiC MESFETs and we have to solve the problems that lead to degradation in SiC bipolar devices. In the process fabrication area we need to improve the activation of p-type implanted dopants in GaN, to achieve large free-hole concentrations and to be able to control the stoicihmetry of epilayer composition (leads to hyperspectral arrays). We need to actively support the development of large area low dislocation density substrates for development of SiC and GaN devices which will allow for increased economies of scale. GaN based LED's have flourished even though dislocation densities are $10^{10}/cm^2$. A five fold reduction in this figure will have a huge impact on the reliability of LEDs, lasers and transistors and will have a dramatic increase in the sensitivity of photodiodes (to achieve near photon-counting!). According to the timeline, see Fig. (1), the threading dislocation density in, for example, bulk or quasi-bulk GaN is now typically $10^6/cm^2$. Improvements should aim to reduce this to $10^5/cm^2$ by 2008 and $10^3/cm^2$ by 2012. Fewer than 10 defects/cm^2 are expected in 2020. A particular challenge for SiC wafers is the availability in larger sizes. Estimates of the timescale to realize different SiC wafer sizes with commercially acceptable quality include 4 inch by 2005 and 8 inch by 2013.

Material Systems to be invested in over the next 16 years

Given the mission, our strategy for compound semiconductor planning highlights critical material systems. The current "hot" material systems are : Gallium nitride (3.7eV); aluminum nitride (6.2eV); indium nitride (0.7 or 1.9eV?); boron nitride (4-7eV); silicon carbide (2.36-3.23eV); zinc oxide (3.4eV). Diamond (Group IV elemental) , even though its not really a compound semiconductor, it is a very important technological material, however, we feel this should be addressed separately under its own white paper. The

fabrication process key developments have to be made in doping and creating electrically conductive diffusion profiles. The number and variety of semiconductor devices seems unlimited but we list here those that will be well suited for fabrication from the above material systems:

Electronics Devices
Bipolar BJT, HBT, Thyrister, GTO
Unipolar JFET, MOSFET, MISFET, MESFET
Diode PN. PIN, Schottky, Avalanche/Zener, Varactor GUNN, IMPATT, TRAPATT, RTD

Opto-Electronic Devices
Receptors PIN, Avalanche photo-diode (APD), Heterojunction Photo Transistor (HPT)
Emitters LED, HB-LED, Laser Diode, VCSEL
Modulators SEED

A look into the future
A timeline for issues relating to technical challenges that we will face are shown below.

Resources
1. The microelectronics advanced research initiative opto-electronics technology roadmap ((MEL-ARI OPTO): http://europa.eu.int/
2. Roadmaps from the National Electronics Manufacturing Initiative (NEMI): http://www.nemi.org
3. Roadmaps from the optoelectronics industry development (OIDA): http://www.oida.org
4. National Compound Semiconductor Roadmap: http://www.onr.navy.mil

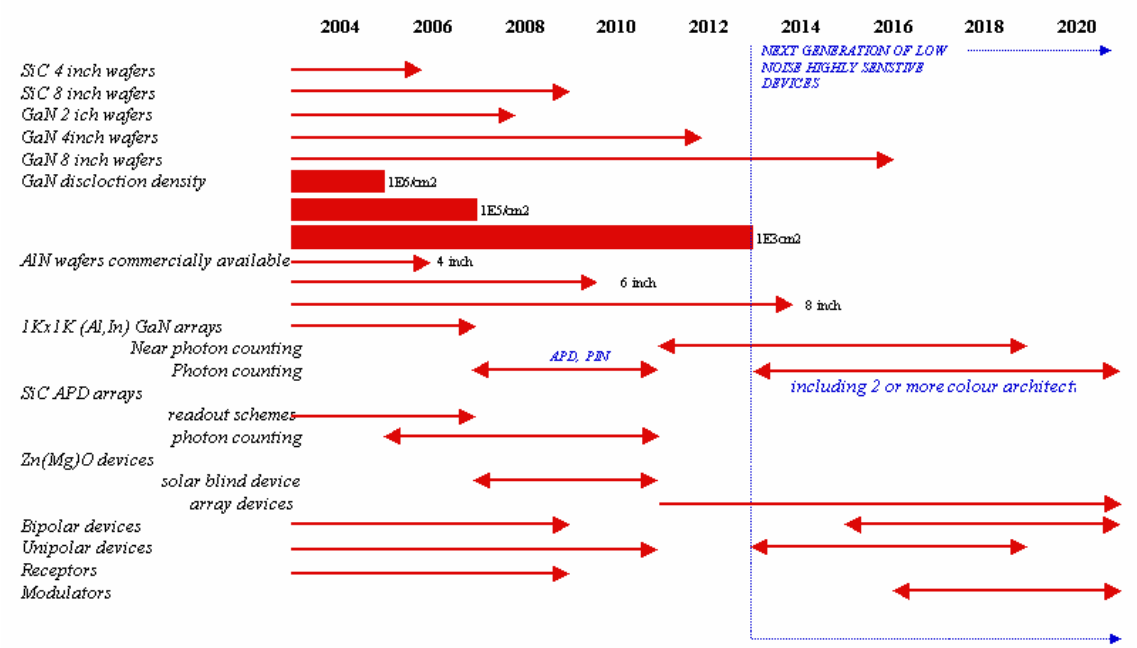

Timeline for key developments

ISSN 1813-2065

Coming

CONFERENCE & SYMPOSIA

Sponsored & Organized by SPIE

SPIE Photomask Technology 28th Annual Symposium
Date(s): 6 - 10 October 2008
Location: Monterey, California, USA
Exhibition Date(s): 7 - 8 October 2008

SPIE Environmental Nanotechnology Online Conference
Date(s): 15 October 2008
Location: Online Conference, USA

SPIE APOC 2008: Asia-Pacific Optical Communications
Date(s): 26 - 30 October 2008
Location: Hangzhou, China

SPIE Lithography Asia - Taiwan
Date(s): 4 - 6 November 2008
Location: Taipei, Taiwan

SPIE Photonics Innovation Summit
Date(s): 6 November 2008
Location: San Francisco, California, USA

International Conference of Optical Instrument and Technology (OIT)
Date(s): 16 - 19 November 2008
Location: Beijing, China

International Symposium on Optomechatronic Technologies
Date(s): 17 - 19 November 2008
Location: San Diego, California, USA

SPIE Asia-Pacific Remote Sensing
Date(s): 17 - 21 November 2008
Location: Noumea, New Caledonia

AOMATT 2008 - 4th International Symposium on Advanced Optical Manufacturing
Date(s): 19 - 21 November 2008
Location: Chengdu, Chengdu, China

SPIE Smart Materials, Nano- and Micro-Smart Systems
Date(s): 9 - 12 December 2008
Location: Melbourne, Australia

IS&T/SPIE Electronic Imaging
Date(s): 18 - 22 January 2009
Location: San Jose, CA, USA

SPIE Photonics West
Date(s): 24 - 29 January 2009
Location: San Jose, California, USA
Exhibition: 27 - 29 January 2009

BiOS: Biomedical Optics
Date(s): 24 - 29 January 2009
Location: San Jose, CA, USA
Exhibition: 24 - 25 January 2009

LASE: Lasers and Applications
Date(s): 24 - 29 January 2009
Location: San Jose, CA, USA
Exhibition: 27 - 29 January 2009

MOEMS-MEMS: Micro and Nanofabrication
Date(s): 24 - 29 January 2009
Location: San Jose, CA, USA
Exhibition: 27 - 29 January 2009

OPTO: Integrated Optoelectronic Devices
Date(s): 24 - 29 January 2009
Location: San Jose, CA, USA
Exhibition: 27 - 29 January 2009

SPIE Medical Imaging
Date(s): 7 - 12 February 2009
Location: Orlando, Florida, USA
Exhibition: 9 - 11 February 2009

SPIE Advanced Lithography
Date(s): 22 - 27 February 2009
Location: San Jose, CA, USA
Exhibition: 24 - 25 February 2009

SPIE Smart Structures and Materials & Nondestructive Evaluation and Health Monitoring
Date(s): 8 - 12 March 2009
Location: San Diego, California, USA

Photomask and NGL Mask Technology XVI
Date(s): 8 - 10 April 2009
Location: Yokohama, Japan

SPIE Defense, Security, and Sensing
Date(s): 13 - 17 April 2009
Location: Orlando, FL, USA
Exhibition: 14 - 16 April 2009

SPIE Europe Optics and Optoelectronics
Date(s): 20 - 24 April 2009
Location: Prague, Czech Republic

ISPDI - International Symposium on Photoelectronic Detection and Imaging
Date(s): 1 - 5 May 2009
Location: Beijing, China

Microtechnologies for the New Millennium
Date(s): 4 - 6 May 2009
Location: Dresden, Germany

SPIE Scanning Microscopy 2009
Date(s): 4 - 7 May 2009
Location: Monterey, California, USA

SPIE Optifab
Date(s): 11 - 14 May 2009
Location: Rochester, New York, USA
Exhibition: 12 - 14 May 2009

International Photodynamic Association World Congress 2009
Date(s): 11 - 15 June 2009
Location: USA

SPIE Europe Optical Metrology
Date(s): 14 - 18 June 2009
Location: Munich, Germany

Effect of Annealing on the Electrical Characteristics of CdO-Si Heterostructure Produced by Plasma-Induced Bonding Technique

Oday A. Hamadi

P. O. Box 55159,
Baghdad 12001,
IRAQ
odayata2001@yahoo.com

In this work, the effect of annealing on the electrical characteristics of the CdO-Si heterojunction produced by plasma-induced bonding technique was studied. The heterojunction was consisting of n-type CdO on a p-type silicon substrate. Results showed reasonable improvement in the electrical characteristics of this heterojunction within a range of annealing temperatures, above which the heterojunction showed degradation in its characteristics. This work produces CdO-Si of much better characteristics than same heterojunctions produced by thermal evaporation technique.

Keywords: CdO-Si structure, Bulk bonding, Heterojunctions, Heat treatment
Received: 12 March 2008, Revised: 25 June 2008, Accepted: 2 July 2008

1. Introduction

Although the main driving force for development of bonding has been production of silicon-on-insulator (SOI), several other high potential applications of bonding have emerged in microelectromechanical systems (MEMS) and as a way of integrating dissimilar crystalline materials. To reach a sufficient level of maturity, bonding procedures need to be optimized and standardized according to the application. Also, bonding requires a high-temperature annealing step after the room temperature joining, to ensure the formation of a strong and uniform bonding. This high temperature annealing is sometimes incompatible with many applications and it may cause material degradation, especially when bonding thermally mismatched materials. Back to the pioneering days, low temperature bonding procedures have been highly desirable [1].

There are many factors governing the bonding behaviour of two surfaces. First, the surfaces must be flat and smooth. Usually it is argued that surfaces can make contact only at some asperities. However, the success of bonding technique has followed the development of modern semiconductor chemical-mechanical polishing (CMP) technology [2]. The semiconductor polishing technology has reached such a level of maturity that, nowadays, commercial silicon wafers have surface roughness in the order of 10^{-10}m. The second parameter governing the ability for bonding is the surface chemical state and surface termination. For most semiconductors, surface preparation and cleaning techniques are well-developed and characterized. However, in silicon technology the surface chemical treatments are more standardized and established processes, as compared to, for example, compound semiconductors [3].

The basic procedure in semiconductor bonding technique starts with mirror-polished surfaces that are cleaned, plasma-activated and given their final surface termination using a combination of chemical treatments [4]. The wafers are then brought together at room temperature and if proper surface conditions apply, the solids will bond spontaneous. After room temperature bonding, a heat treatment at elevated temperature is performed to strengthen the interface bonding [5]. Typical bonding technique procedures are fully compatible with microelectronic process technologies, offering several advantages both in available processing equipment and possible applications [6].

One of the great potentials of the bonding approach is the integration of dissimilar materials. Integration of dissimilar semiconductor by heteroepitaxial growth is hampered by the difference in lattice constants. Particularly, combining III-V compounds semiconductors with highly developed silicon circuits has been pursued in recent years with the goal to incorporate photonic and high-speed devices with advanced silicon technology [7].

When the solids have been bonded together at room temperature usually the interaction, or bonding energy, is relatively weak. Therefore, a heat treatment is performed to increase the bond-strength. The annealing enhances out-diffusion

of interface trapped molecules and desorption of chemisorbed surface atoms, such as hydrogen [8]. At the same time the annealing activates formation of covalent bonds between the bonded surfaces, like solid-to-solid bonding in the case of hydrophobic bonding. The thermal treatment used to increase the bond-strength can, unfortunately, also cause severe problems in bonding technique. For instance, when bonding dissimilar materials, the thermal mismatch induced high stresses in the material. High temperature annealing also restricts the use of metal patterns and can cause diffusion of dopants [9].

Generally, the bonding requires a high-temperature annealing step to ensure the formation of strong bonding between solids, i.e. to form covalent bonds. In silicon-to-silicon bonding usually an annealing above 1000°C is required, and in bonding involving compound semiconductors, the annealing is usually performed above 600°C. Such a high-temperature annealing is incompatible with many applications. Particularly, pre-structured wafers that already contain temperature-sensitive structures cannot be exposed to the high-temperature annealing. The high-temperature annealing also induces material degradation. It can cause broadening of diffusion layers. When bonding dissimilar materials, annealing at high temperatures would induce large thermal stress due to the difference in thermal expansion coefficients [10].

In this work, the annealing of CdO-Si structure produced by low-temperature plasma-induced bonding was performed and its effect on the electrical characteristics of this structure was studied.

2. Experimental Work

The experimental details of preparing samples were presented in Ref. [11]. High purity (99.999) (100)-oriented p-type silicon wafers of 500μm thickness and 3Ω.cm resistivity were used in this work. Also, high purity (99.999) cadmium oxide (CdO) was used to form 350μm-thick samples. Both samples, Si and CdO, were washed with distilled water then rinsed in ethanol and subjected to ultrasonic waves for 10 minutes, then dried by hot air. The silicon samples were then cleaned with HF for 5 minutes to remove any residual oxides which have existed on their surfaces. Both samples were softly grinded and polished to obtain flat surfaces. Then, these samples were rinsed in ethanol to remove acids then dried to be ready for processing.

However, the bonding is very weak at room temperature and after low-temperature annealing because of the hydrogen-terminated surface. A high-temperature annealing above 520°C is necessary to desorb hydrogen from surface and enable a covalent bonding. The difference in thermal expansion between CdO and Si will induce high mechanical stress in the material when annealing the bonded samples at high-temperatures. The thermal stress degrades the material by generating defects. It can also cause cracks and completely debond. The main degradation occurs in CdO since Si is a mechanically stronger material. The samples were subjected to heating up to 800°C. The sample was heated for 5 minutes then left to return to its initial temperature within the same period of time.

3. Results and Discussion

The effect of annealing temperature on the ideality factor and spectral responsivity of the prepared CdO-Si heterojunctions was first introduced within the range (400-800)°C in order to determine the optimum value of annealing temperature, as shown in Fig. (1) and (2). Temperature of 600°C is shown to be the optimum value and this is in good agreement with the published works.

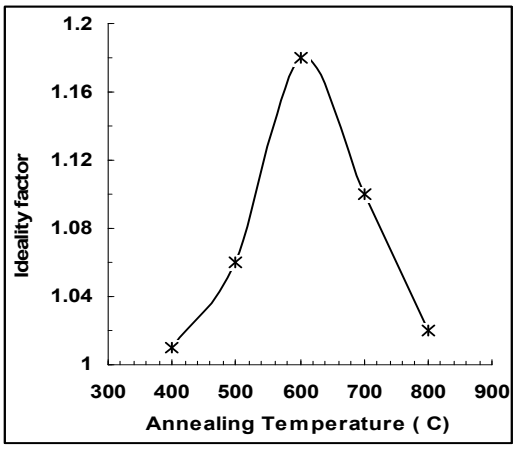

Fig. (1) The ideality factor of the CdO-Si heterojunction at different annealing temperatures

Wafer bonded p-n hetrojunction characteristics are heavily affected by the non-ideal interface. However, a substantial improvement of wafer bonded p-n heterojunctions characteristics is usually obtained by shifting the p-n transition away from the bonded interface, either by high temperature annealing [12] or by implantation [13-14]. Alternatively, the p-n heterojunction, formed under UHV conditions and low temperatures results in an ideality factor no more than 1.18, indicates low recombination at the interface. Bonding p-n heterojunction in ambient air and subsequent high temperature annealing was seen to yield high recombination near the bonded

interface. An ideality factor of 2 was obtained and low minority carrier lifetime [15].

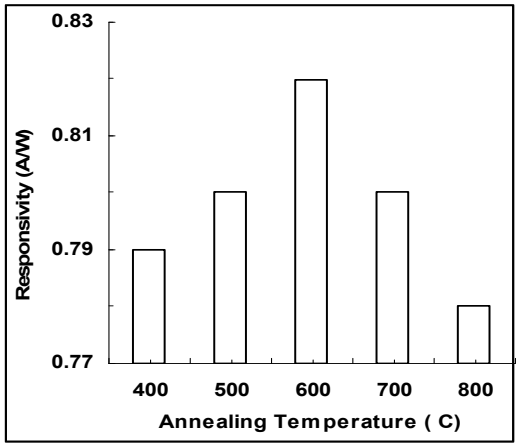

Fig. (2) The spectral responsivity of the CdO-Si heterojunction at different annealing temperatures

Fig. (3) shows the I-V characteristics of bonded p-n Si-CdO heterojunction. As shown, the dark current is about 50μA and the forward current is uniformly linear. The illumination current in the reverse biasing reaches a maximum of about 180μA. The bonded interface is often avoided in the electrically active region of the electronic device. However, the recombination centers of the defective bonded interface are used to control the minority carrier lifetime in power devices. These characteristics are typically enhanced compared to results obtained by other techniques [16].

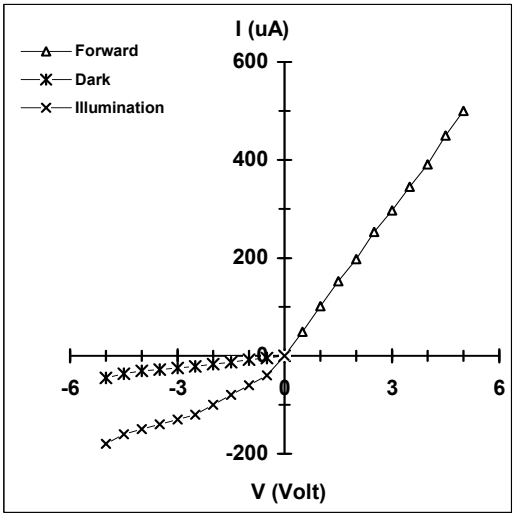

Fig. (3) The I-V characteristics in dark and light for the CdO-Si heterojunction annealed at 600°C

In order to introduce the nature of the anisotype CdO-Si heterojunction, the C-V measurements were performed in the reverse biasing and results are presented in Fig. (4). The built-in potential was determined for the CdO-Si heterojunction to be about 0.9eV.

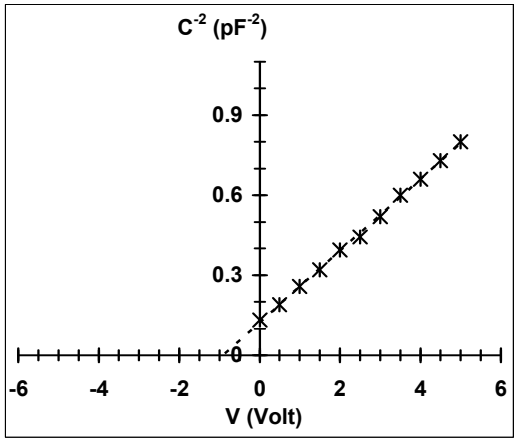

Fig. (4) The C-V characteristics of the CdO-Si heterojunction annealed at 600°C. The value of V_{bi} is about 0.9eV

The spectral responsivity of the CdO-Si heterojunction was determined as a function of wavelength as shown in Fig. (5). This heterojunction responds in the 550-900nm range much more than in the range below 550nm. This cheap technique presents an advantage to produce good photodetectors for the wavelengths more than 550nm.

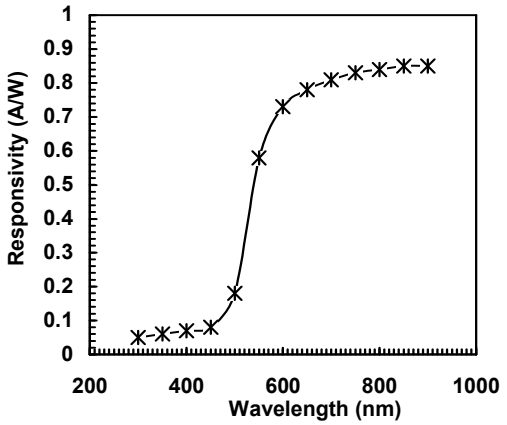

Fig. (5) The spectral responsivity of the CdO-Si heterojunction annealed at 600°C

Integration of CdO and Si has attracted much interest since the unique properties in each material can be combined in devices or systems, such as CdO-based piezoelectric devices and optoelectronics components. The epitaxial growth of CdO on Si substrate is hampered by the difference between the lattice constants of the materials. However, using bonding for the integration, the lattice-mismatch becomes no obstacle. Unfortunately, there is a large difference in thermal expansion between CdO and Si. When bonding solids of dissimilar materials and annealing at elevated temperatures, the thermal mismatch will induce high thermal stress in the material [17].

In each material system, nature has imposed a set of physical properties, such as mobility, optical absorption, resistivity, thermal and mechanical properties. For a given application, the optimal properties may not reside in a single material but in a variety of dissimilar materials. A specific case is to combine compound semiconductor that have direct band gap and high mobility with Si that is extensively used in microelectronic applications.

The applications for integrating CdO with Si can be divided into three categories, were each category has its own constraint on interface and material properties [18].

(1) The unique properties of each material are combined in devices to reach optimal performance. An avalanche photodetector, for instance, has two functions absorption of light and conversion of light into an electrical signal. Therefore, the CdO was bonded to Si substrate since the CdO has high light absorption at NIR wavelengths while Si has a much higher electron/hole ionization rate leading to higher avalanche multiplication efficiency [19].

(2) Integration of CdO piezoelectric and high-speed devices with Si microelectronic circuits. Optical interconnections are very desirable since they can overcome the electrical interconnect bandwidth bottleneck. Optical communication links finds application in both rack-to-rack, board-to-board and intra and interchip connections [20]. The integration of CdO devices with Si VLSI circuits may be especially advantageous since Si is transparent at NIR wavelengths. Therefore, optical communications can take place within Si bulk, which facilitates back-surface integration of micro-optics such as beam reflectors. The most straightforward approach, flip-chip bonding, which is currently used to form hybrid optoelectronic IC's, suffers from an inherent throughput limit when multiple optical nodes exist in each die. Furthermore, thermal stress and non-planar surface profiles present additional difficulties for vertical integrated optoelectronics [21-22].

(3) Si as substrate for CdO relieves the strain from CdO substrate industry. Compound semiconductor industry has implied the need for wafers with large diameters. This is much more evident in present electronic applications than in optoelectronics. However, the increment in wafer-size has not followed the same progress and there are major concerns about the up-scaling of CdO wafer dimensions [23]. CdO has several disadvantages since it is fairly immature and the crystal quality is less than the more mature Si and GaAs technologies. Also, CdO wafers are more brittle and available only in small sizes. By implementing bonding techniques, Si could be introduced as a substrate for CdO-based materials. Si wafers offers several advantages such as its low-cost, large area, mechanical strength and high thermal conductivity.

4. Conclusions

A CdO-Si heterojunction was produced by plasma-induced bonding techniques. Electrical measurements showed reasonable enhancement in the heterojunction characteristics compared to that produced by another techniques. Annealing of the prepared samples improve the electrical characteristics much more. Despite the complexity imposed by the plasma processing system, production of heterojunctions with such enhanced characteristics has advantages of low cost and large size devices.

References

[1] Y. Zhou et al., *IEEE Photon. Lett.*, 12 (2000) 110.
[2] D.L. Mathine, *IEEE J. Selec. Top. Quantum Electron.*, 3 (1997) 952.
[3] R. Stengl, K.-Y- Ahn, U. Gösele, *Jpn. J. Appl. Phys.* 27 (1988) L2364.
[4] F.P. Widdershoven, J. Haisma, J. Naus, *J. Appl. Phys.* 68 (1990) 6253.
[5] J. Steinkirchner et al., *Adv. Mater.* 7 (1995) 662.
[6] H. Takagi et al., *Appl. Phys. Lett.* 68 (1996) 2222.
[7] U. Gösele et al., *Appl. Phys. Lett.*, 67 (1995) 3614.
[8] A. Berthold, B. Jakoby, M. J. Vellekoop, *Sensors & Actuators*, A68 (1998) 410.
[9] Q.-Y. Tong, W. J. Kim, T.-H. Lee, U. Gösele, *Electrochem. Solid State Lett.* 1 (1998) 52.
[10] G. Krauter, A. Schumacher, U. Gösele, T. Jaworek, G. Wagner, *Adv. Mater.* 9 (1997) 417.
[11] O.A. Hamadi, *J. Mater. Design Appl. (JMDA)*, 222 (2007) 1-7.
[12] B. Levine et al., *Appl. Phys. Lett.* 75 (1999) 2141.
[13] A. Black et al., *IEEE J. Select. Topics Quantum Electron.*, 3 (1997) 943.
[14] H. Wada, H. Sasaki, T. Kamijoh, *Solid Stat. Electron.,* 43 (1999) 1655.
[15] D. Kikuchi, S. C. Adachi, *Mater. Sci. Eng.* ***B***, 76 (2000) 133.
[16] L.A. Zazzera, J. F. Moulder, *J. Electrochem. Soc.*, 136 (1989) 484.
[17] F.A. Kish et al., *Appl. Phys. Lett.*, 67 (1995) 260.
[18] C. Parkes et al., *Ext. Abs. Electrochem. Soc. Fall. Mtg.,* 91-92 (1991) 724.

[19] A. Hawkins, W. Wu, P. Abraham, K. Streubel, J. E. Bowers, *Appl. Phys. Lett.*, 70 (1996) 303.
[20] H. Yamaguchi, S. Fujino, T. Hattori, Y. A. Hamakawa, *Jpn. J. Appl. Phys.,* 34 (1995) L199.
[21] D. Pasquariello and K. Hjort, *J. Electrochem. Soc.*, 147 (2000) 2343-2346.
[22] H. Ohashi et al., *Int. Electron. Develop. Meet. Tech. Dig.*, (1987) 678.
[23] D.S. Wuu, R. H. Horng, M. K. Lee, *J. Appl. Phys.* 68(7) (1990) 3338.

This article was reviewed at Department of Mechanical Engineering, University of Strathclyde, Glasgow, UK, Dept. of Electronics Engineering, Kyungwon University, Kyunggi-do, KOREA, and School of Applied Sciences, University of Technology, Baghdad, IRAQ

THE 2009 IAENG INTERNATIONAL CONFERENCE ON COMPUTER SCIENCE

19-21 March, 2009, Hong Kong

http://www.iaeng.org/IMECS2009/ICCS2009.html

The conference ICCS'09 is held under the International MultiConference of Engineers and Computer Scientists 2009. The IMECS 2009 is organized by the International Association of Engineers (IAENG), and serves as good platforms for the engineering community members to meet with each other and to exchange ideas. The last conference in 2008 has attracted a total of over one thousand participants from over 50 countries.

All submitted papers will be under peer review and accepted papers will be published in the conference proceeding. The abstracts will be indexed and available at major academic databases. The accepted papers will also be considered for publication in the special issues of the journal Engineering Letters, in IAENG journals and in edited books. Revised and expanded version of the selected papers may also be included as book chapters in the standalone edited books under the framework of cooperation between IAENG and Springer. For reference, the following IAENG post conference edited books, Trends in Intelligent Systems and Computer Engineering, Advances in Communication Systems and Electrical Engineering, and Advances in Industrial Engineering and Operations Research, have been published by Springer.

Important Dates:
Draft Manuscript submission deadline:
12 December, 2008
Camera-Ready papers & Pre-registration due:
10 January, 2009
ICCS 2009: **18-20 March, 2009**

Submission:
ICCS 2009 is now accepting manuscript submissions. Prospective authors are invited to submit their draft paper in full paper (any appropriate style) to **imecs@iaeng.org** by 12 December, 2008. The submitted file can be in MS Word format, PS format, or PDF formats.

The first page of the draft paper should include:
(1) Title of the paper;
(2) Name, affiliation and e-mail address for each author;
(3) A maximum of 5 keywords of the paper.

Also, the name of the conference that the paper is being submitted to should be stated in the email.

The topics of the ICCS'09 include, but not limited to, the following:
- **Theoretical computer science:**
- **Hardware:**
- **Computer systems organization:**
- **Computing methodologies:**
- **Computer applications:**

More details about the IMECS 2009 can be found at:
http://www.iaeng.org/IMECS2009/index.html

Recent Progress in ORGANIC Nanostructure Devices

Written by
Stephen Forrest
Advanced Technology Center for Photonics and Optoelectronic Materials
Princeton University
Princeton, NJ, U.S.A

Scientific Drivers

A primary motivation for the extensive research over the last several years concentrating on the growth and physics of organic thin film nanostructures is their very real potential for use in applications that are not accessible to more conventional, inorganic semiconductors. The recent demonstration of efficient electroluminescence from organic thin film devices promises to transform the flat panel display industry (Tang and VanSlyke 1987; Burrows and Forrest 1994; Burroughes et al. 1990), with the potential of replacing liquid crystal displays with an entirely new generation of efficient, emissive, full color flat panels based on light-emitting organic devices. In more recent developments, organic thin films are showing promise for use as thin film transistors (TFTs) (Dodabalapur et al. 1995; Garnier et al. 1990; Garnier et al. 1997), which might eventually replace amorphous or polysilicon TFTs currently used in the back planes of active matrix liquid crystal displays (AMLCD). These new developments also must be placed in the context of long efforts and progress that has been directed at employing organic thin films for solar energy conversion (Wohrle and Meissner 1991; Tang 1986) and in sensors of various kinds. Finally, vacuum-deposited OMCs have also been proposed as materials with large second or third order optical nonlinearities (Lam et al. 1991; Agranovich et al. 1995; Maruyama et al. 1995; Fang et al. 1993; Leegwater and Mukamel 1992; Wang and Mukamel 1994; Dubovsky and Mukamel 1992; Mukamel et al. 1994), or large ((Burroughes et al. 1990). There are, in addition, many, somewhat less conventional uses of organic thin films deposited in vacuum, including waveguides and optical couplers (Zang et al. 1991; Zang and Forrest 1992; Taylor et al. 1997), organic/inorganic photodetectors (So and Forrest 1989; Forrest et al. 1982), and lasers.

The primary attraction of organic molecular nanostructures is their potential low cost and the extreme flexibility that the device engineer has in choosing a material whose properties have been specifically tailored to meet the needs of a particular application. The materials are easily integrated with conventional semiconductor devices, thereby providing additional functionality to existing photonic circuits and components.

The potentials of organic molecular nanostructures, however, must be balanced against the problems that have traditionally impeded acceptance of organics for use in active electronic or optoelectronic device applications, including unstable device characteristics; sensitivity to adverse environments (e.g., temperature, humidity, oxygen, etc.); non-ideal metal/organic contacts; and lack of reproducibility of material composition, purity, and fabrication conditions.

It is clear that the ultrahigh vacuum environment characteristic of organic thin film deposition processes can provide the necessary material purity and structural and chemical reproducibility necessary in modern, high performance optoelectronic device applications. While the costs and complexities associated with ultrahigh vacuum (UHV) deposition processes may offset the attractive (but possibly misleading) "simplicity" often attributed to organic-based devices, it is clear that the performance advantages of such structures outweigh these apparent disadvantages. Furthermore, while purity and structural precision are key to the ultimate success of all optoelectronic device technologies, it is not clear how sophisticated the deposition system must be to achieve acceptable device performance. At this point, vacuum deposition serves as the most powerful tool for investigating the detailed growth and physical characteristics of organic nanostructure devices, and hence will ultimately be able to address questions regarding the need for UHV in the production of practical display,

transistor, NLO, or other molecular organic thin film device applications.
As a background for understanding the current status of organic nanostructures R&D, below is a compilation of some of the best results for organic thin film devices reported to date:

1. ***Solar Cells*** (Tang 1986; Forrest and So 1988): Highest power conversion efficiency for bilayer organic cells: 1-2%. Challenges that remain include insufficient efficiency to be practical. Also, stability of the devices is inadequate for power generation applications.

2. ***Organic Light-Emitting Devices*** *(OLEDs)* (Tang and Van Slyke 1987; Burrows and Forrest 1994; Burrows et al. 1996; Dodabalapur et al. 1994; Tang et al. 1989): These devices are positioning themselves to replace LCDs in several display applications. Some performance characteristics include high brightness (1,000 times brighter than CRT elements) and high efficiency (1-3%). Full color has been demonstrated, but saturated color is not obtainable at all corners of the color palate (R, G, and B), and stability of the devices exceeds 10,000 hrs at video brightness. Several challenges yet remain before widespread acceptance of OLEDs will occur. These include the ability to make fully color tunable devices at low cost and to manufacture very thin structures with an acceptable yield. While the operational lifetime of some devices (particularly green emitters) is quite good, other colors (e.g., red) do not have the same high performance and stability attributes. However, there are numerous groups worldwide pursuing OLED technology, and Pioneer intends to bring out a display based on OLEDs in early 1998.

3. ***Organic Thin Film Transistors*** (Dodabalapur et al. 1995; Garnier et al. 1990; de Leeuw et al. 1997; Dodabalapur, Torsi, and Katz 1995; Lin et al. 1997, 143): Remarkable progress in TFTs based on organic materials has been made in the last couple of years. In particular, pentacene-based organic transistors have resulted in channel mobilities equal to that of amorphous Si (~1cm^2/V-s), threshold voltages V_T~0V, and on/off current ratios ~10^6, albeit not necessarily all on the same device. In addition, circuits consisting of 10 to 20 polymer-based TFTs have also recently been reported (de Leeuw et al. 1997). These results represent major breakthroughs in organic electronics, although many challenges remain. Nevertheless, significant economic drivers exist for ultralow-cost electronics for identification cards, low density memories, display backplanes, etc., which may provide the driving force necessary to bring these devices into widespread use.
These are only three examples of where organic nanostructures are finding application due to the advanced state of their development. As in the case of all immature technologies, there are still significant barriers to their adoption in the commercial world. However, for the first time, active organic nanostructures appear to be on the verge of transforming a large number of optical and electronic applications.

References

Agranovich, V.M., G.C. LaRocca and F. Bassani, *Chem. Phys. Lett.*, 247 (1995) 355.
Burroughes, J.H., D.D.C. Bradley, A.R. Brown, R.N. Marks, K. Mackay, R.H. Friend, P.L. Burns and A.B. Holmes, *Nature,* 347 (1990) 539.
Burrows, P.E. and S.R. Forrest, *Appl. Phys. Lett.* 64 (1994) 2285.
Burrows, P.E., S.R. Forrest, S.P. Sibley and M.E. Thompson, *Appl. Phys. Lett.*, 69 (1996) 2959.
de Leeuw, D.M., A.R. Brown, M. Matters, K. Chmil and C.M. Hart, Paper H3.5 (1997) p.144. FETs constructed from precursor-route conjugated polymers, San Francisco.
Dodabalapur, A., H.E. Katz, L. Torsi and R.C. Haddon, *Science,* 269 (1995) 1560.
Dodabalapur, A., L.J. Rothberg and T.M. Miller, *Appl. Phys. Lett.*, 65 (1994) 2308.
Dodabalapur, A., L. Torsi and H.E. Katz, *Science,* 268 (1995) 270.
Dubovsky, O. and S. Mukamel, *J. Chem. Phys.*, 15 (1992) 417.
Fang, S., K. Kohama, H. Hoshi and Y. Maruyama, *Japan. J. Appl. Phys.*, 32 (1993) L1418.
Forrest, S.R., M.L. Kaplan, P.H. Schmidt, W.L. Feldmann and E. Yanowski, *Appl. Phys. Lett.*, 90 (1982).
Forrest, S.R. and F.F. So, *J. Appl. Phys.*, 64 (1988) 399.
Garnier, F., G. Horowitz, D. Fichou and A. Yassar, *Supramolec. Sci.*, 4 (1997) 155.
Garnier, F., G. Horowitz, X. Peng and D. Fichou, *Adv. Mater.*, 2 (1990).
Lam, J.F., S.R. Forrest and G.L. Tangonan, *Phys. Rev. Lett.*, 66 (1991) 1614.
Leegwater, J.A. and S. Mukamel, *Phys. Rev. A,* 46 (1992) 452.
Lin, Y.-Y., D.J. Gundlach and T.N. Jackson, MRS Spring Meeting 1997, San Francisco, CA.
Maruyama, Y., H. Hoshi, S.L. Fang and K. Kohama, *Synthetic Metals,* 71 (1995) 1653.
Mukamel, S., A. Takahashi, H.X. Huang and G. Chen, *Science,* 266 (1994) 250.
So, F.F. and S.R. Forrest, *IEEE Trans. Electron. Dev.*, 36 (1989) 66.
Tang, C. W, *Appl. Phys. Lett.*, 48 (1986) 183.
Tang, C.W. and S. A. VanSlyke, *Appl. Phys. Lett.*, 51 (1987) 913.
Tang, C.W., S.A. VanSlyke and C.H. Chen, *J. Appl. Phys.*, 65 (1989) 3610.
Taylor, R.B., P.E. Burrows and S.R. Forrest, *IEEE Photonics Technology Lett.,* 9 (1997) 365.
Wang, N. and S. Mukamel, *Chem. Phys. Lett.*, 231 (1994) 373.
Wohrle, D. and D. Meissner, *Adv. Mater.*, 3 (1991) 129.
Zang, D.Y. and S.R. Forrest, *IEEE Photon. Technol. Lett.*, 4 (1992) 365.
Zang, D.Y., Y.Q. Shi, F.F. So, S.R. Forrest and W.H. Steier, *Appl. Phys. Lett.*, 58 (1991) 562-564.

ISSN 1813-2065

IRAQI JOURNAL OF APPLIED PHYSICS

" INSTRUCTIONS TO AUTHORS "

A new Iraqi specialized quarterly periodical dedicated to publishing original papers, letters and reviews in:

Applied & Nonlinear Optics	Electronic Materials & Devices	Quantum Physics & Spectroscopy
Applied Mechanics & Thermodynamics	Laser Physics & Applications	Semiconductors & Optoelectronics
Digital & Optical Communications	Plasma Physics & Applications	Solid State Physics & Applications

CONTRIBUTIONS

Contributions to be published in this journal should be original research works, i.e., those not already published or submitted for publication elsewhere, individual papers or letters to editor.

SUBMISSION OF MANUSCRIPTS

Manuscripts should be submitted to the editor at the mailing address:

Iraqi Journal of Applied Physics
Managing Editor
P. O. Box 55259, Baghdad 12001, IRAQ
irq_appl_phys@yahoo.com

Iraqi Journal of Applied Physics
Editor-In-Chief
P. O. Box 55259, Baghdad 12001, IRAQ
editor_ijap@yahoo.co.uk

MANUSCRIPTS

Two copies with soft copy on a compact disc (CD) should be submitted to Editor in the following configuration:

- Double-spaced one-side A4 size with 2.5 cm margins of all sides
- 12pt Times New Roman font
- Letters should not exceed 5 pages, papers no more 20 pages and reviews are up to author.
- Manuscripts presented in English only are accepted.
- Authors confirm affiliations, addresses and emails. Email is necessary for correspondences.
- English abstract not exceed 150 words
- 4 keywords (at least) should be maintained on (PACS preferred)
- Author(s) should express all quantities in SI units
- Equations should be written in equation form (italic and symbolic)
- Figures and Tables should be separated from text
- Figures and diagrams can be submitted in colors for assessment and they will be returned to authors after provide printable copies
- Charts should be indicated by the software used for
- Only original or high-resolution scanner photos are accepted
- References should be written in titles, full-name authors, names of publications, years, volumes, issues and pages (from-to)

PROOFS

Authors will receive proofs of papers and are requested to return one corrected hard copy with a WORD copy on a compact disc (CD). New materials inserted in the original text without Editor permission may cause rejection of paper.

COPYRIGHT FORM

Author(s) will be asked to transfer copyrights of the article to the Journal soon after acceptance of it. This will ensure the widest possible dissemination of information.

OFFPRINTS

Authors will receive offprints free of charge and any additional offprints can be ordered.

SUBSCRIPTION AND ORDERS

Annual fees (4 issues per year) of subscription are:

- 50 000 Iraqi dinars for individuals and establishments inside Iraq.
- 50 US$ for individuals and establishments abroad.

Fees are reduced by 25% for I.S.A.R.E.S.T. members. Orders of issues can be submitted by contacting the editor-in-chief or editorial secretary to maintain the address of issue delivery and payment way.

THE IRAQI JOURNAL OF APPLIED PHYSICS
EDITORIAL BOARD

COPYRIGHY RELEASE

Iraqi Journal of Applied Physics (IJAP)

We, the undersigned, the author/authors of the article titled

……
……
……
……
……
……

that is presented to the Iraqi Journal of Applied Physics (IJAP) for publication, declare that we have neither taken part or full text from any published work by others, nor presented or published it elsewhere in any other journal. We also declare transferring copyrights and conduct of this article to the Iraqi Journal of Applied Physics (IJAP) after accepting it for publication.

The authors will keep the following rights:

1. **Possession of the article such as patent rights.**
2. **Free of charge use of the article or part of it in any future work by the authors such as books and lecture notes without referring to the IJAP.**
3. **Republishing the article for any personal purposes of the authors after taking journal permission.**

To be signed by all authors:

Signature:……..date: ……..

Printed name: ……

Signature:……..date: ……..

Printed name: ……..

Signature:……..date: ……..

Printed name: ……..

Correspondence address:

……
……
……
Address:……
……
……
Telephone:……..email: ……..

Note: Please complete and sign this form and mail it to the below address with your manuscript

The Iraqi Journal of Applied Physics,
P. O. Box 55259, Baghdad 12001, IRAQ
Email: editor_ijap@yahoo.co.uk, Tel.: +964-7901274190

IRAQI JOURNAL OF APPLIED PHYSICS

CONTENTS